Journal of Sound and Vibration (1998) **217**(2), 351–386
Article No. sv981806

ESTIMATING THE VIBRATIONAL ENERGY CHARACTERISTICS OF AN ELASTIC STRUCTURE VIA THE INPUT IMPEDANCE AND MOBILITY

YU. I. BOBROVNITSKII

Laboratory of Structural Acoustics, *Mechanical Engineering Research Institute of Russian Academy of Sciences*, *M. Kharitonievsky* 4, 101830 *Moscow*, *Russian Federation*

(*Received* 8 *October* 1997, *and in final form* 26 *June* 1988)

Several equations are proposed which relate the time-average energy of a forced vibrating linear structure to the structure input impedance and mobility. When the structure is driven at one point, the equations allow one to obtain the kinetic and potential energy, loss factor and other energy characteristics by the most economic way: without measuring or computing the response all over the structure and using only the data measured at the driving point. Computer simulation examples with typical structures show that the equations provide reliable estimates in the range of low and middle frequencies.

1. INTRODUCTION

In experimental mechanics and acoustics, an important problem is that of minimizing the measured data necessary for characterizing a mechanical system. It follows not only from the natural requirement of economy but also from the practical restrictions: for many engineering structures, installation of sensors and, hence, the direct measurement of the needed structural characteristics is undesirable or even impossible.

In structural dynamics, Bolotin [1] was probably the first who rigorously formulated and solved one such problem called the problem of planning the vibration measurements on structures: for a structure vibrating under a random load, he gave several criteria (such as the minimum condition number) for how to choose the amount and co-ordinates of the measurement points necessary to reconstruct the statistical moments of the time-spatial random vibration field. In the last few years, a similar problem has been discussed in the literature on modal analysis, the problem of planning modal tests, consisting of the selection of excitation positions and response measurement locations which are the best for the model (mostly, a FE-model) validation [2]. One more such problem, called the field reconstruction problem, was formulated and studied in reference [3]; it consists of reconstructing the vibration displacement and stress fields inside an

0022–460X/98/420351 + 36 $30.00/0

elastic solid from the displacement amplitudes measured on a part of its boundary surface. There are other publications containing attempts to extract the maximum information from the minimum experimental data—see, e.g., references [4–6].

In the present paper, an extreme problem of this type is considered. It consists of finding the time-average energy characteristics of a vibrating mechanical structure driven at one point if only the data measured at this single point are given. As is shown in the paper, the problem has no exact solution: mathematically one can find only the power dissipated in the structure and the Lagrange function (the difference between the kinetic and potential energy). Other energy characteristics of the structure cannot, in the general case, be expressed through the measurements at one point. However, it turns out that, for finite and not highly damped structures, simple approximate equations can be obtained which give rather accurate estimates for all the energy characteristics of the structure. Derivation and analysis of these equations is the main objective of the present paper.

The key result of this work is the equation which relates the total vibration energy of a structure to the derivative of the input impedance (or mobility) of the structure with respect to frequency. This equation is mathematically correct for finite lossless structures [7]. Here, it is applied to structures with arbitrary damping. Several computer simulation examples illustrate the accuracy and the range of validity of the estimates thus obtained. Some of the results have been presented in reference [8]. They can be useful in developing techniques for analysis of vibration in complex practical systems which at present are urgently required [2]. In particular, they can provide a technique for direct measurement of some energetic parameters of subsystems used in the prediction methods based on the energy balance equations—see, e.g., reference [9].

2. ENERGY RELATIONS FOR AN *n*DOF-SYSTEM DRIVEN AT ONE POINT

2.1. FORMULATION OF THE PROBLEM

The following problem is considered: a finite linear structure is driven at one point by a harmonic force; find all the time-average energy characteristics of the structure (kinetic energy, potential energy, loss factor and others), if only the complex amplitudes of the force and the velocity response at the driving point, f and v, are given (measured). The question is, thus, in finding the energy characteristics without measuring or computing the response over the whole structure.

2.2. *n*DOF-MODEL

It is assumed that the structure is modelled by a linear mechanical system with n degrees of freedom (nDOF) whose forced vibration of angular frequency ω is described by a set of algebraic equations

$$\mathbf{f} = \mathbf{Z}\mathbf{v} = (\mathbf{R} + \mathrm{i}\mathbf{X})\mathbf{v}, \tag{1}$$

where $\mathbf{f} = [f_1, \ldots, f_n]^T$ and $\mathbf{v} = [v_1, \ldots, v_n]^T$ are n-vectors of the complex amplitudes of external forces and the velocity response of the system, $\mathbf{Z}$ is the full impedance $n \times n$-matrix, and superscript T means transposition. The time dependent factor $\exp(-i\omega t)$ is implied. (A list of symbols is given in Appendix C.) The real part of the impedance matrix, the resistance matrix $\mathbf{R}$, and its imaginary part or reactance $\mathbf{X}$ relate to the system parameter matrices as

$$\mathbf{R} = \mathbf{C} + (1/\omega)\mathbf{H}, \qquad \mathbf{X} = (1/\omega)\mathbf{K} - \omega\mathbf{M}. \tag{2}$$

Here, $\mathbf{C}$ and $\mathbf{H}$ are the $n \times n$-matrices of viscous and hysteretric damping, $\mathbf{K}$ and $\mathbf{M}$ are the static stiffness and mass $n \times n$-matrices. All the square matrices in equations (1) and (2), except $\mathbf{Z}$, are assumed to be real-valued and symmetric. The impedance matrix $\mathbf{Z}$ is complex and symmetric. The damping matrices, $\mathbf{C}$ and $\mathbf{H}$, are not necessarily proportional to $\mathbf{K}$ and/or $\mathbf{M}$. The nDOF-system and equations (1) and (2) thus model a rather general class of mechanical structures.

The following time-average energy characteristics of the system will be of further interest: the complex power flow into the system

$$\mathbf{F} = \mathbf{I} + i\mathbf{Q} = \tfrac{1}{2}\mathbf{v}^*\mathbf{f}, \tag{3}$$

of which the real and imaginary parts are the active and reactive power flow; dissipated power

$$\Phi = \tfrac{1}{2}\mathbf{v}^*\mathbf{R}\mathbf{v}; \tag{4}$$

kinetic and potential energies

$$T = \tfrac{1}{4}\mathbf{v}^*\mathbf{M}\mathbf{v}, \qquad U = (1/4\omega^2)\mathbf{v}^*\mathbf{K}\mathbf{v}; \tag{5}$$

total energy and Lagrange function

$$E = T + U, \qquad L = T - U; \tag{6}$$

loss factor of the system

$$\eta = \Phi/\omega E, \tag{7}$$

defined at each frequency as the ratio of the energy dissipated during one period of oscillation to the time-average total energy of the system. The asterisk denotes the Hermitian conjugate, i.e., transposition plus complex conjugate. Though the velocity amplitude vector $\mathbf{v}$ is complex, the dissipated power (4) as well as the energy characteristics (5), (6) are real (and positive) since the resistance, mass, and stiffness matrices are assumed symmetric.

The problem posed in section 2.1 can be reformulated for the nDOF-system driven at one, say the first, DOF ($f_1 = f, f_2 = \cdots = f_n = 0$), as follows: find the characteristics (4)–(7) if the complex amplitude $f_1 = f$ and the velocity response component $v_1 = v$ are given, while the velocity vector components $v_2, \ldots, v_n$ and the matrices $\mathbf{M}$, $\mathbf{K}$, $\mathbf{C}$, $\mathbf{H}$ remain unavailable.

2.3. EXACT RELATIONS

Using the amplitudes f and v, one can immediately compute the input impedance $z(\omega)$ and input mobility $y(\omega)$ at the driving point,

$$z(\omega) = f/v, \qquad y(\omega) = v/f, \tag{8}$$

as functions of frequency, as well as the active and reactive power flows

$$I = \tfrac{1}{2}\,\mathrm{Re}\,(\bar{v}f,) \qquad Q = \tfrac{1}{2}\,\mathrm{Im}\,(\bar{v}f). \tag{9}$$

To find the energy characteristics (4)–(7), one has to obtain equations which relate them to the known quantities (8) and (9). Two such equations can be derived by substituting equations (1) and (2) into equation (3) and comparing the result with equations (4)–(6). These are

$$I = \Phi, \qquad Q = -2\omega L. \tag{10, 11}$$

Equation (10) is equivalent to the energy conservation law: the power flow into the structure is equal to the dissipated power. Equation (11) gives one more physical interpretation of the reactive power flow Q: it is a measure of closeness of the structure to a resonance. (Note that the time-average potential energy is equal to the time-average kinetic energy only at the natural frequencies.)

From equations (10) and (11) one can find two of the needed energy characteristics of the structure—the dissipated power and Lagrange function:

$$\Phi = \tfrac{1}{2}|v|^2\,\mathrm{Re}\,[z(\omega)], \qquad L = -\tfrac{1}{4}|v|^2\,\mathrm{Im}\,[z(\omega)/\omega]. \tag{12}$$

Unfortunately, that is all that can be calculated exactly via the input data (8) and (9). For other energy characteristics, only approximate values can be found.

2.4. ESTIMATES VIA THE INPUT IMPEDANCE

For the time-average total energy E, the following estimate via the input impedance is proposed here:

$$E \cong -\tfrac{1}{4}|v|^2\,\mathrm{Im}\,[\partial z(\omega)/\partial\omega]. \tag{13}$$

This equation gives exact values for the total energy of lossless structures for which the input impedance is a purely imaginary quantity. It was rigorously proved for this case in reference [7]; its derivation together with a brief review of related literature is presented in Appendix A. For damped structures, equation (13) is approximate. Accuracy of the approximation depends upon the amount of damping in the structure: the smaller the damping, the lower the approximation error. The examples given in section 3 show that equation (13) gives rather realistic estimates for the total energy in many practical cases at low and middle frequencies.

Combining equations (12) and (13), one can easily obtain the following estimates for the time-average kinetic and potential energy separately,

$$T \cong -\tfrac{1}{8}|v|^2\,\mathrm{Im}\left[\frac{\partial z(\omega)}{\partial\omega} + \frac{z(\omega)}{\omega}\right], \qquad U \cong -\tfrac{1}{8}|v|^2\,\mathrm{Im}\left[\frac{\partial z(\omega)}{\partial\omega} - \frac{z(\omega)}{\omega}\right], \tag{14, 15}$$

and for the loss factor (7) of the system

$$\eta \cong -2 \operatorname{Re}\left[\frac{z(\omega)}{\omega}\right] \Big/ \operatorname{Im}\left[\frac{\partial z(\omega)}{\partial \omega}\right]. \tag{16}$$

2.5. ESTIMATES VIA THE INPUT MOBILITY

As is shown in Appendix A, the total energy of a lossless nDOF-system relates to the input mobility in just the same manner as it does to the input impedance—see equation (A11). Therefore, the estimates, similar to equations (13)–(16), for the energy characteristics via the input mobility can be easily derived. By repeating the procedure of the preceding section with the input impedance replaced by the input mobility, the following equations can be written:

$$\Phi = \tfrac{1}{2}|f|^2 \operatorname{Re}[y(\omega)], \qquad E \cong -\tfrac{1}{4}|f|^2 \operatorname{Im}[\partial y(\omega)/\partial \omega], \tag{17, 18}$$

$$T \cong -\tfrac{1}{8}|f|^2 \operatorname{Im}\left[\frac{\partial y(\omega)}{\partial \omega} - \frac{y(\omega)}{\omega}\right], \tag{19}$$

$$U \cong -\tfrac{1}{8}|f|^2 \operatorname{Im}\left[\frac{\partial y(\omega)}{\partial \omega} + \frac{y(\omega)}{\omega}\right], \tag{20}$$

$$\eta \cong -2 \operatorname{Re}\left[\frac{y(\omega)}{\omega}\right] \Big/ \operatorname{Im}\left[\frac{\partial y(\omega)}{\partial \omega}\right]. \tag{21}$$

Equations (12)–(21) solve the posed problem. They allow one to obtain all the time-average energy characteristics of a forced vibrating finite mechanical structure from the measurements only at one single point, i.e., without measuring or computing the responses all over the structure: one needs for this to measure the input impedance or mobility and the amplitude of the velocity response (or force) at the driving point.

3. COMPUTER SIMULATION EXAMPLES

To illustrate the accuracy and the range of validity of the estimates obtained, three vibrating structures are studied in this section: nDOF-system with viscous damping ($n = 2$), and two continuous structures with hysteretic damping—a longitudinally vibrating uniform rod (one dimensional structure), and flexurally vibrating rectangular plate (two dimensional structure).

3.1. 2DOF-SYSTEM

This system consists of two masses m_1 and m_2, two springs k_1 and k_2, and two dashpots c_1 and c_2—as shown in Figure 1. The external load is applied to the lower

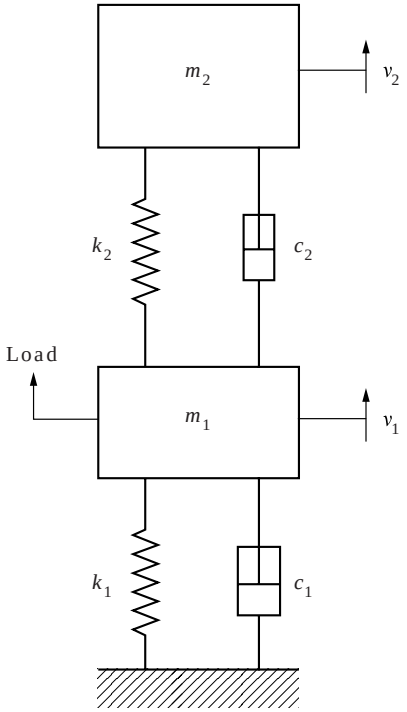

Figure 1. Two-degree-of-freedom-system.

mass m_1. The response of the system is described by equations (1) and (2) with the system matrices

$$\mathbf{M} = \begin{bmatrix} m_1 & 0 \\ 0 & m_2 \end{bmatrix}, \qquad \mathbf{K} = \begin{bmatrix} k_1 + k_2 & -k_2 \\ -k_2 & k_2 \end{bmatrix}, \qquad \mathbf{C} = \begin{bmatrix} c_1 + c_2 & -c_2 \\ -c_2 & c_2 \end{bmatrix}.$$

The energy characteristics (4), (5) are

$$\Phi = \tfrac{1}{2}c_1|v_1|^2 + \tfrac{1}{2}c_2|v_2 - v_1|^2, \qquad T = \tfrac{1}{4}m_1|v_1|^2 + \tfrac{1}{4}m_2|v_2|^2,$$
$$U = \tfrac{1}{4}k_1|u_1|^2 + \tfrac{1}{4}k_2|u_2 - u_1|^2, \tag{22}$$

where u_j and $v_j = -\mathrm{i}\omega u_j$ are the complex amplitudes of the mass displacement and velocity. Some results of computation are presented in Figures 2–8. They correspond to the system with the following parameters (22): $k_1 = k_2 = k$; $m_1 = 4m_2$; the loss factor of the first contour $m_1 - c_1 - k_1$ is equal to $\eta_1 = c_1/m_1\omega_1 = 0{\cdot}2$ and the loss factor of the second contour $m_2 - c_2 - k_2$ is equal to $\eta_2 = c_2/m_2\omega_2 = 0{\cdot}05$ where $\omega_1^2 = k_1/m_1$ and $\omega_2^2 = k_2/m_2$ are the partial eigenfrequencies of the two uncoupled contours.

Two cases of the external load are considered separately—force loading and kinematic excitation. In the first case, the driving force remains constant at all frequencies: $f_1(\omega) = f = \text{const}$. Kinematic excitation means in general that the amplitude of displacement, velocity or acceleration remain constant independently of the driven system. In our case, the velocity amplitude of the first mass is kept

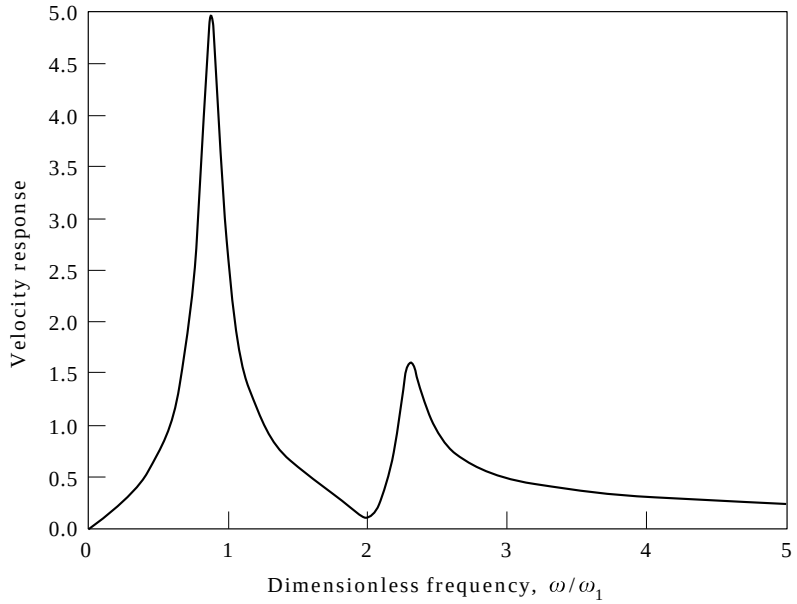

Figure 2. Velocity amplitude of the driven mass of a 2DOF-system under force excitation.

up constant at all frequencies: $v_1(\omega) = v_0 = \text{const}$; never mind what force is needed for this.

3.1.1. *Force excitation*

The velocity response $|v_1|$ of the first mass normalized with $|f|/m_1\omega_1$ is presented in Figure 2 as a function of frequency. One can see two resonances at the system eigenfrequencies $\omega/\omega_1 = 0{\cdot}87$ and $2{\cdot}3$, and one anti-resonance in between at the frequency $\omega/\omega_1 = 2{\cdot}0$. This is the partial eigenfrequency of the second contour which acts here as a dynamic silencer in relation to the first mass. Figures 3–6 depict the energy characteristics of the 2DOF-system vibrating under the force excitation. The kinetic, potential and dissipated energies as well as their combinations L and E are normalized with the quantity $|f|^2/4k$. The solid line curves in Figures 3–6 show the exact values of the characteristics (22) while the dotted lines correspond to the estimates computed by using equations (12)–(16) or (17)–(21). As expected and clearly seen in Figure 3, there is a full coincidence between the exact values and the values computed by equation (12) for the time-average Lagrange function and the energy dissipated in the system during one period. Figure 4 shows the total energy of the system as a function of frequency. It is apparent from Figure 4(a) that the estimate through the input impedance, according to equation (13), is practically indistinguishable from the exact values in all the frequency range except the vicinity of the anti-resonance frequency where it even becomes negative. Alternatively, the estimate using the input mobility according to equation (18) gives erroneous results at the resonance frequencies (negative values), though at the anti-resonance and all other frequencies (see Figure 4(b)) the results coincide with the exact ones.

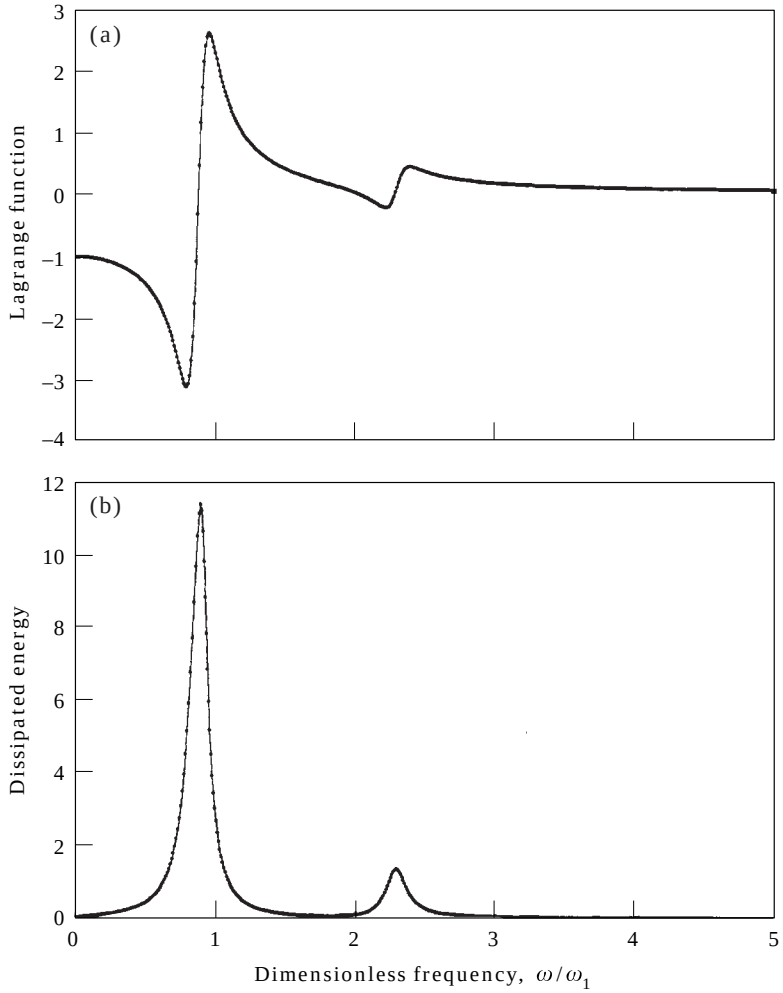

Figure 3. Time-average Lagrange function (a) and the energy dissipated during one period (b) in a 2DOF-system excited by a force.

Similar behavior is demonstrated by the kinetic energy (Figure 5(a)), the potential energy (Figure 5(b)), and the loss factor (Figure 6). The estimates (14)–(16) via the input impedance are very good at all frequencies with the exception of a small frequency band around the anti-resonance frequency. The estimates (19)–(21) via the input mobility (not shown in Figures 5 and 6), on the contrary, fail at the resonance frequencies and give good approximation in the rest of the frequency range (as in Figure 4(b)). It can be concluded from Figures 3–6 that, for a system under force loading, the estimates (12)–(16) via the input impedance give much better results than the estimates (17)–(21) which use the input mobility.

3.1.2. *Kinematic excitation*

In this case, the velocity amplitude of the first mass is assumed to be constant v_0 at all frequencies. The amplitude of the velocity response of the second mass

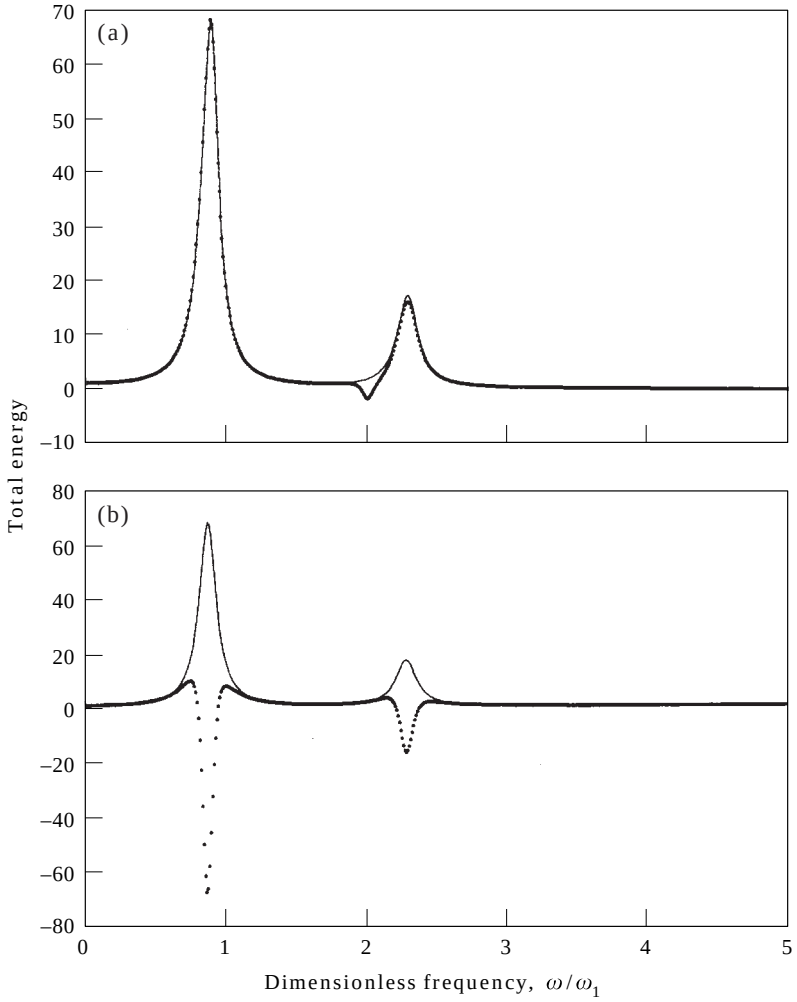

Figure 4. The time-average total energy of the forced vibrating 2DOF-system as a function of frequency: exact values (solid lines) and the values estimated (dotted lines) via the input impedance (a) and the input mobility (b).

normalized with $|v_0|$ is shown in Figure 7. The only peak is seen here at the frequency $\omega/\omega_1 = 2$ which corresponds to the anti-resonance, as was established in the previous section (compare with Figure 2), while the natural frequencies of the system, $\omega/\omega_1 = 0{\cdot}87$ and $2{\cdot}3$, that is to say resonance frequencies, do not display in the response. This feature is intrinsic to a kinematic loading. Nevertheless, the energy estimates under study hold their properties in this case too: the estimate via the input impedance fails only at the anti-resonance frequency and the estimate through the input mobility gives good results everywhere but at the natural (resonance) frequencies. This is clearly seen in Figure 8. Comparing Figures 4 and 8 that show the frequency dependence of total energy of the 2DOF-system in these two cases, one comes to the following conclusion.

When a mechanical system is subject to a *force excitation* in a broad frequency band, its response is determined by the resonances and most of the vibrational

energy is concentrated near the resonance frequencies. Consequently, the energy estimates via the input impedance give the best results, since the erroneous values of these estimates near the anti-resonance frequencies contribute only a little to the overall response level.

On the other hand, when the system is subject to a broad band *kinematic excitation*, the total energy of its response is located mostly near the anti-resonance frequencies, in which case the energy estimates based on the use of the input mobility give the best results. In the next section it is shown that this conclusion also holds for continuous mechanical systems with hysteretic damping.

3.2. A LONGITUDINALLY VIBRATING ROD

Consider a thin straight uniform rod of a finite length l executing longitudinal vibrations under the action of an external harmonic load applied to the left end

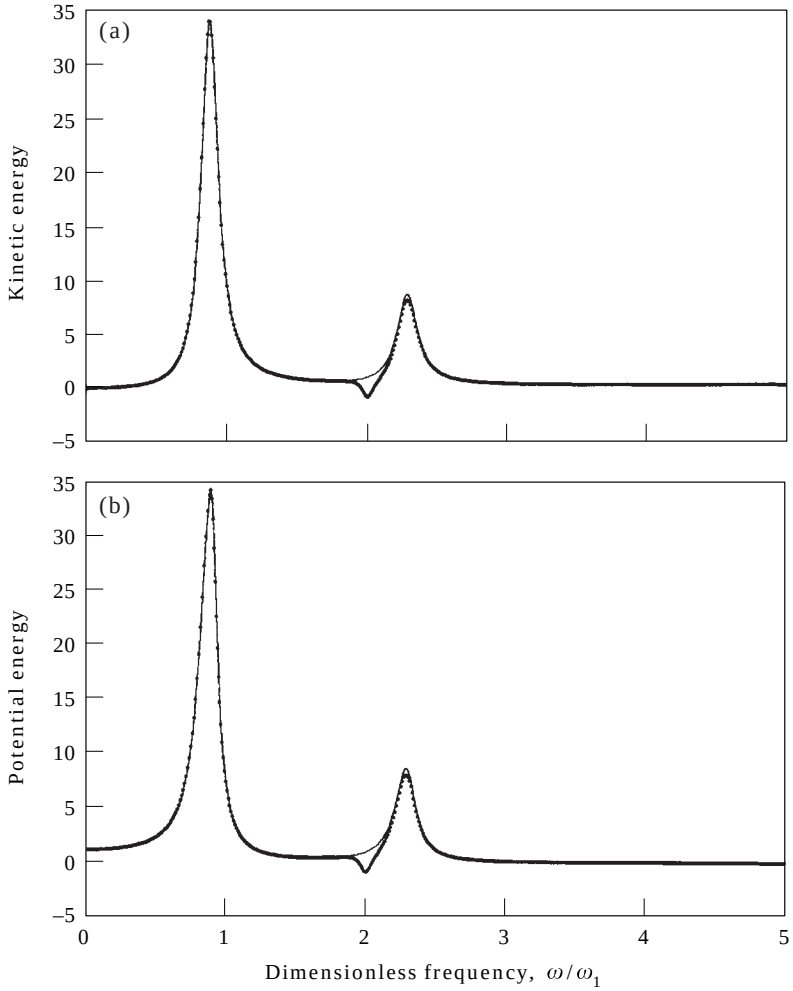

Figure 5. The time-average kinetic (a) and potential (b) energy of the forced vibrating 2DOF-system: exact values (solid lines) and the values estimated via the input impedance (dotted lines).

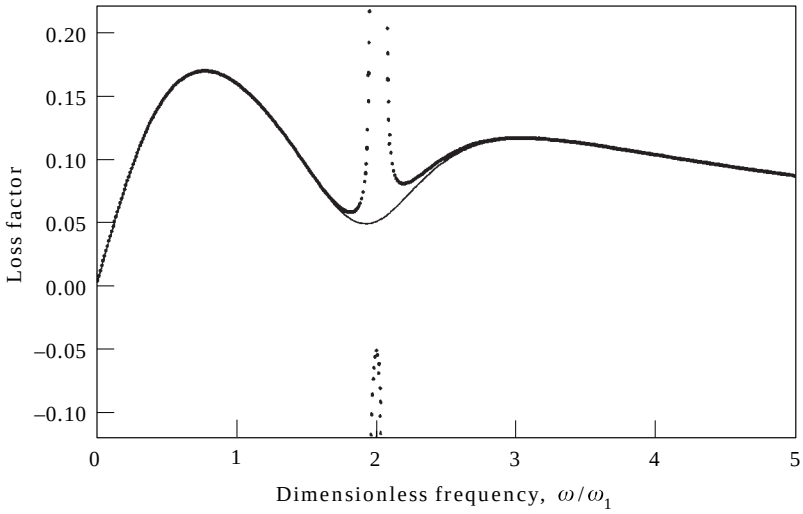

Figure 6. The loss factor of the forced vibrating 2DOF-system as a function of frequency: exact values (solid lines) and the values estimated via the input impedance (dots).

$x = 0$—see Figure 9(a). It is assumed that the vibrations are governed by the classical equation of Bernoulli [10]: $E_c S u''(x) + \rho S \omega^2 u(x) = 0$ with a complex Young's modulus

$$E_c = E_0(1 - \mathrm{i}\eta_0), \tag{23}$$

where η_0 is the material loss factor independent of frequency, ρ is the material density and S is the cross-sectional area. The right end of the rod is free of tension. The boundary condition at the left end depends on the type of the load.

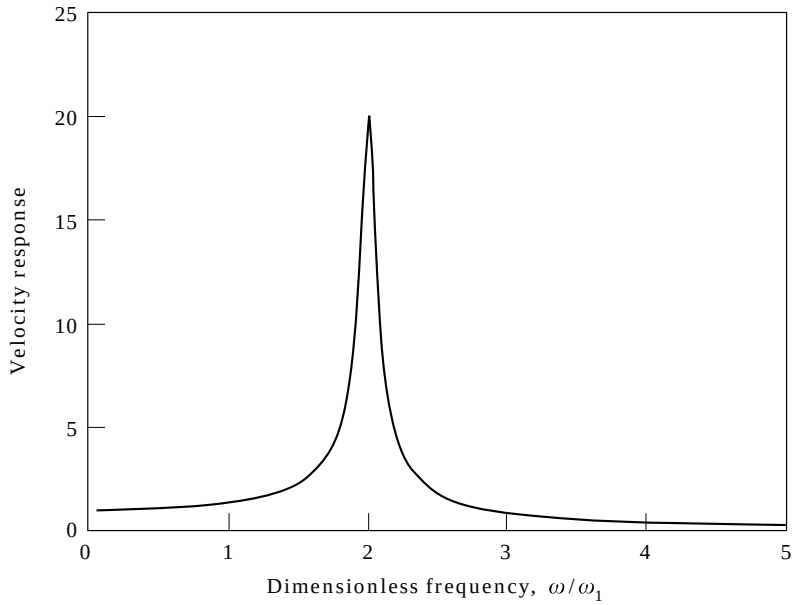

Figure 7. Velocity response of the undriven mass of the 2DOF-system under kinematic excitation.

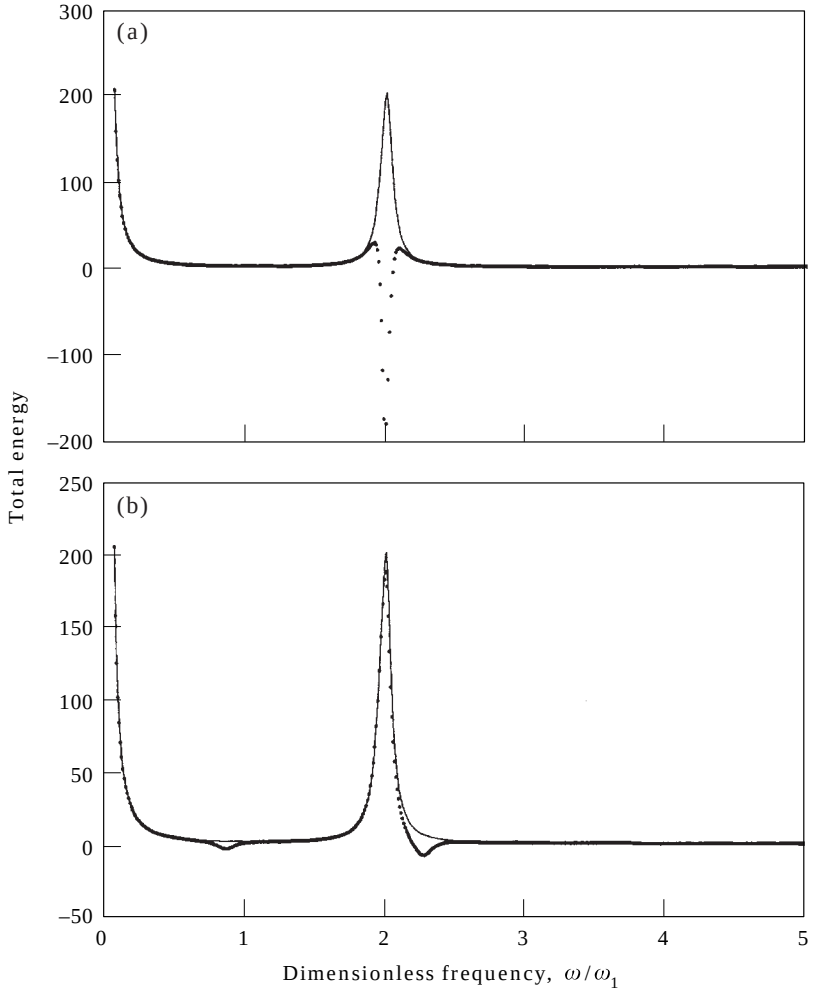

Figure 8. The time-average total energy of the kinematically excited 2DOF-system as a function of frequency: exact values (solid lines) and the values estimated (dots) via the input impedance (a) and the input mobility (b).

The problem has a simple analytical solution [10]. In the case when the rod's left end is loaded by a force of a constant complex amplitude f, the velocity response is

$$v(\xi) = \frac{\mathrm{i}f \cos\left[\Omega(1-\xi)\right]}{z_0 \sin \Omega}, \tag{24}$$

where $z_0 = (E_c \rho S^2)^{1/2}$ is the so-called characteristic impedance, $\xi = x/l$ and

$$\Omega = \Omega_0/\sqrt{1 - \mathrm{i}\eta_0}, \qquad \Omega_0 = \omega l \sqrt{\rho/E_0}, \tag{25}$$

is the dimensionless frequency.

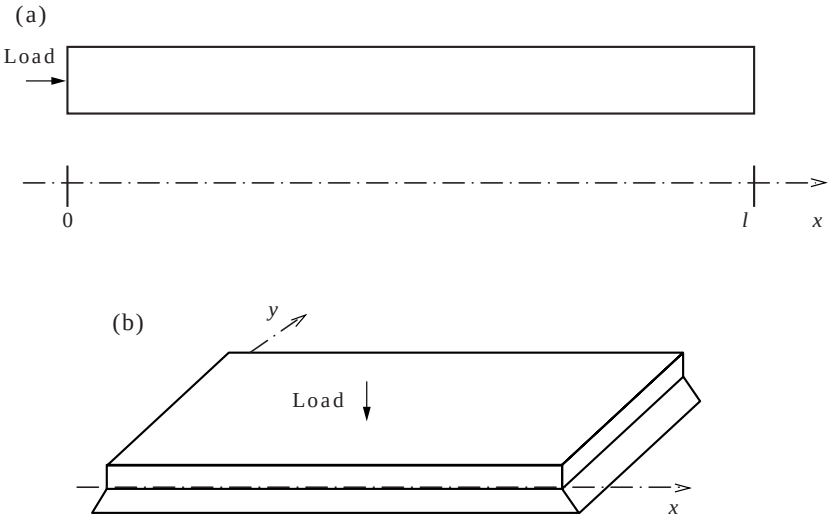

Figure 9. A rod driven at the left end (a) and a simply supported rectangular plate driven at one point.

When the rod is excited kinematically, i.e., when the left end vibrates at all frequencies with a constant velocity amplitude v_0, the rod response is

$$v(\xi) = v_0 \frac{\cos[\Omega(1-\xi)]}{\cos \Omega}. \tag{26}$$

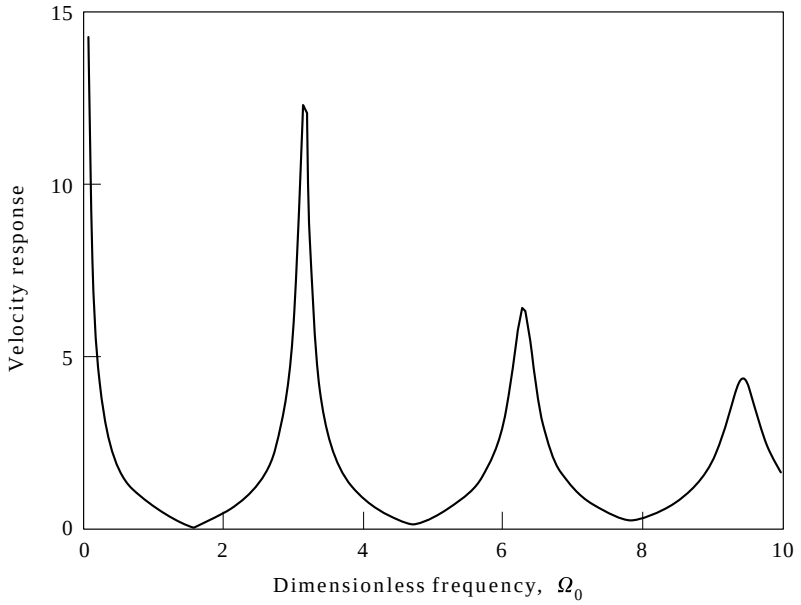

Figure 10. Velocity response of the left rod end.

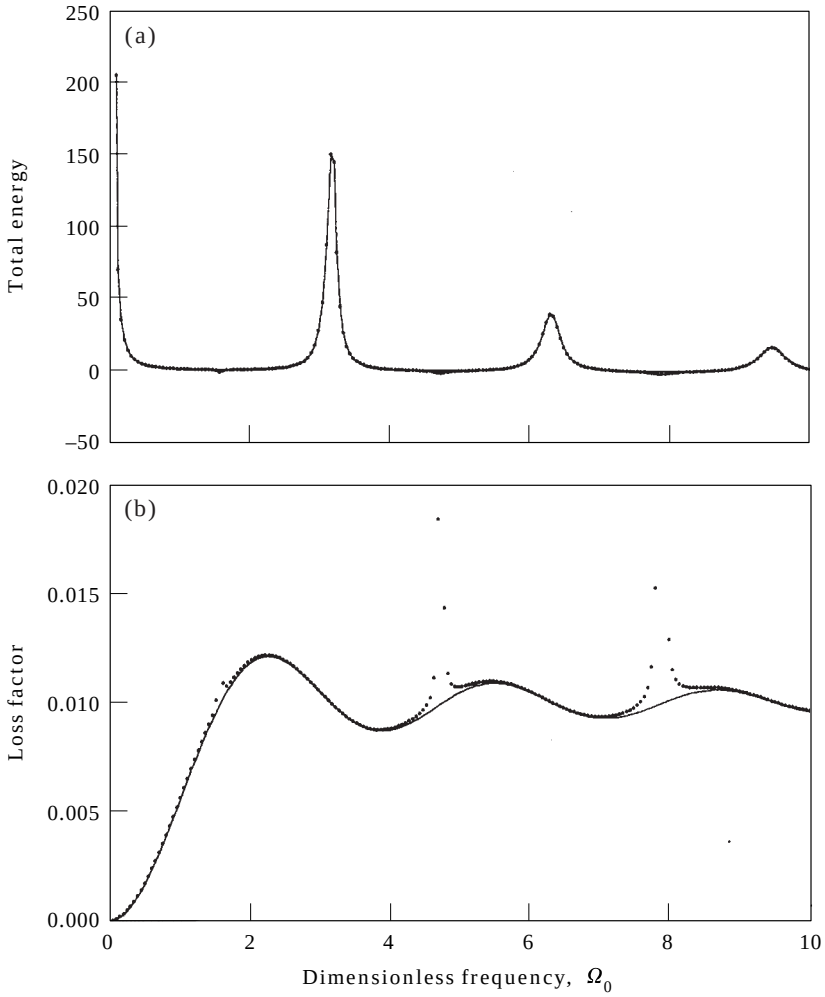

Figure 11. The time-average total energy (a) and loss factor (b) of the forced vibrating rod: exact values (solid lines) and estimates via the input impedance (dots); the material loss factor η_0 is equal to 0·05 (a) and 0·01 (b).

The input impedance of the left end is equal to

$$z(\omega) = \frac{f}{v(0)} = -\mathrm{i}z_0 \frac{\sin \Omega}{\cos \Omega}, \tag{27}$$

and the input mobility is the inverse of this expression. The exact values of the energy characteristics (4)–(7), calculated by integration over the rod length, as well as their estimates (12)–(21), can also be easily expressed in the analytical form but are omitted for brevity. Instead, in Figures 10–14 some of them are presented graphically.

The results for the force excited rod are presented in Figures 10–12. The velocity response of the driving point normalized with the quantity $|f/z_0|$ is shown in Figure 10, where the horizontal axis corresponds to the dimensionless longitudinal wavenumber (25) proportional to frequency, and the loss factor (23) of the rod

material is equal to $\eta_0 = 0{\cdot}05$. The response consists of a number of peaks (resonances) at the natural frequencies $\Omega_0 = \pi m$ of the free–free rod which are separated by the anti-resonances with minimum response amplitudes. The frequencies of the anti-resonances are equal to the natural frequencies of the rod with the fixed left end: $\Omega_0 = \pi n + \pi/2$. It should be noted that a similar form is obtained for the response function at the right end or other cross-section of the forced excited rod. The energy characteristics for this case of loading are presented in Figures 11 and 12. The total energy (Figure 11(a)), as well as the kinetic and potential energy (Figure 12), have the same maxima and minima as the velocity response in Figure 10. Again, the estimates (12)–(16) using the input impedance (dotted lines in Figures 11 and 12) provide excellent agreement with the exact values at all frequencies, with the exception of small frequency bands around the anti-resonance frequencies. The accuracy of the estimates for the kinetic and

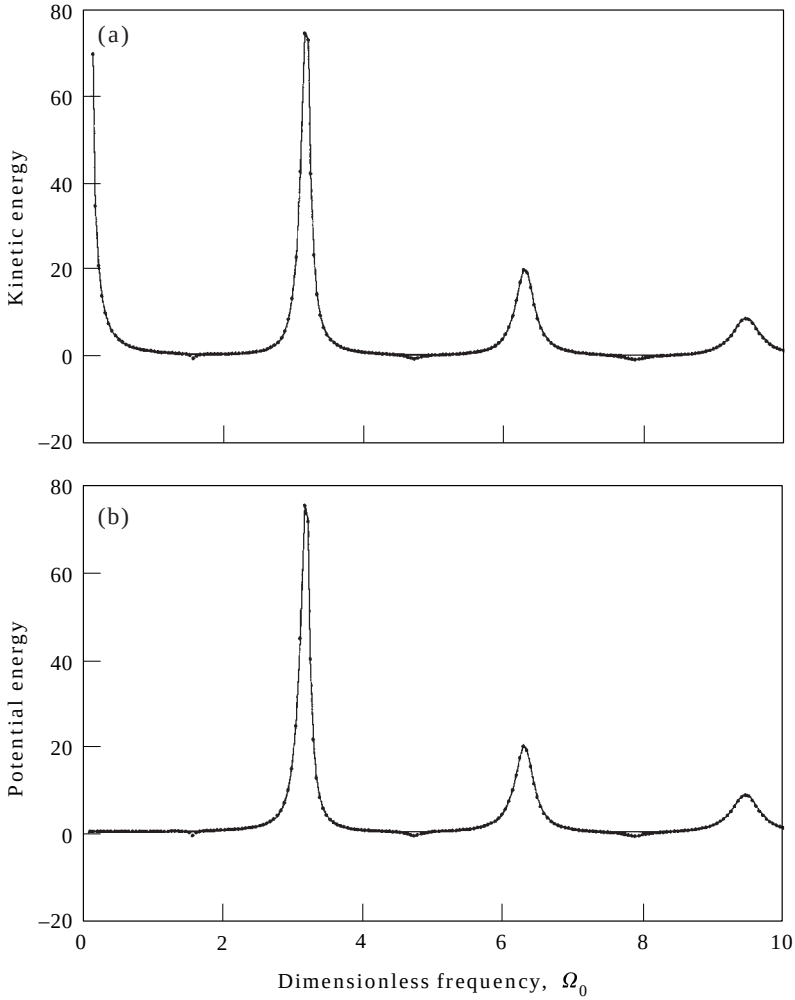

Figure 12. The time-average kinetic (a) and potential (b) energy of the forced vibrating rod: exact values (solid lines) and estimates via the input impedance (dots); $\eta_0 = 0{\cdot}05$.

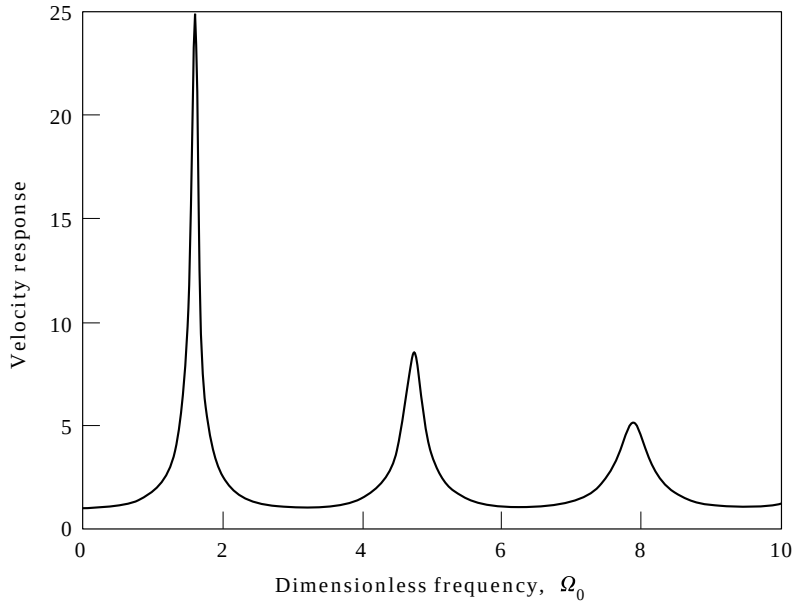

Figure 13. The velocity response of the right end of the rod kinematically excited at the left end; $\eta_0 = 0{\cdot}05$.

potential energy is of the same order as that for the total energy—see equations (14) and (15). As for the estimates (17)–(21), their behavior is just similar to that demonstrated in Figure 4(b). Note that the energy characteristics in Figures 11 and 12 are normalized with the quantity $|f^2/4(E_c S/l)|$.

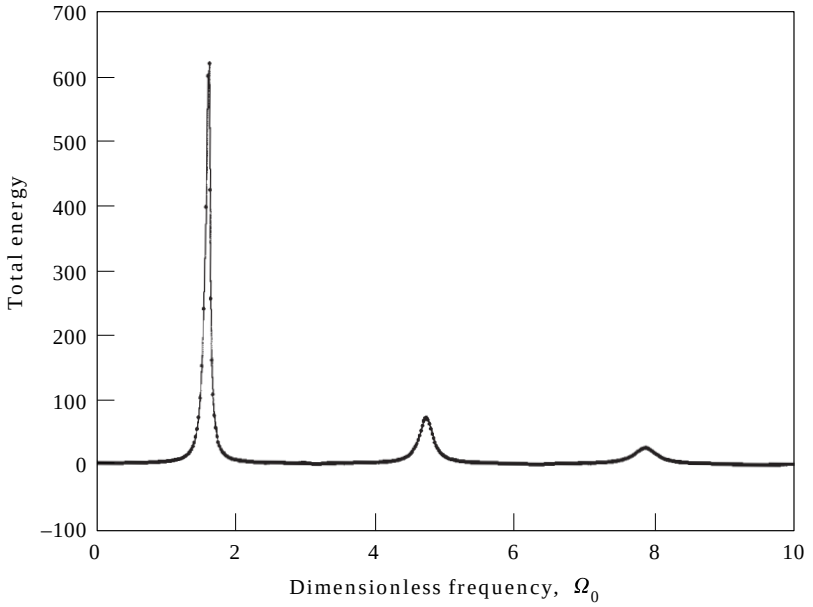

Figure 14. The time-average total energy of the kinematically excited rod: exact values (solid lines) and estimates via the input mobility (dotted lines); $\eta_0 = 0{\cdot}05$.

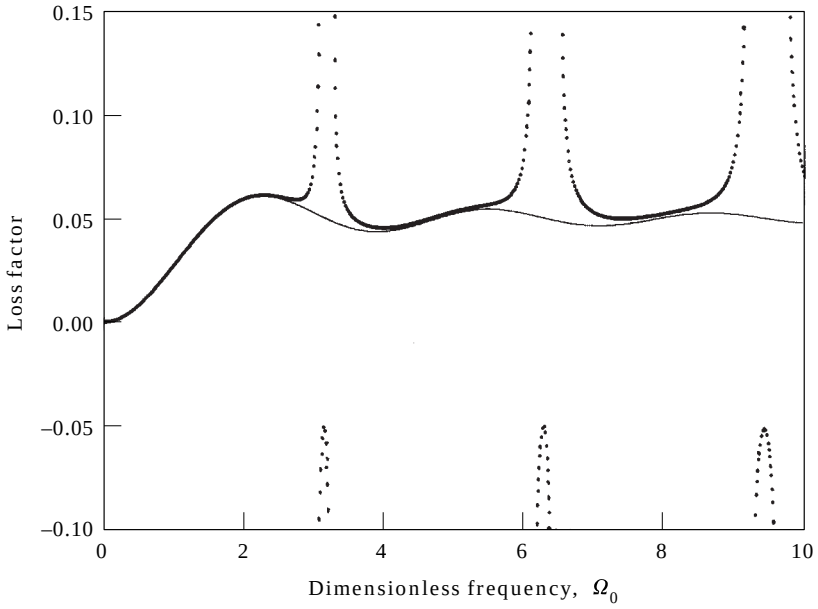

Figure 15. The loss factor of the kinematically excited rod: exact values (solid lines) and estimates via the input mobility (dots); the material loss factor is equal to 0·05.

When the rod is excited kinematically, the resonances and anti-resonances change their roles. As seen in Figure 13, the velocity response (26) of the right rod's end normalized with $|v_0|$, has maxima just at the anti-resonance frequencies $\Omega_0 = \pi n + \pi/2$ and minima at the resonance frequencies $\Omega_0 = \pi m$. Therefore, for obtaining the best estimation of the total energy and other characteristics, one has to use the input mobility. Figure 14 confirms this: the exact values (solid lines) and the estimates via the input mobility (dots) are almost identical in all the frequency range. The same high accuracy is obtained for the estimates via mobility for the kinetic and potential energies. However, for the loss factor of the rod, the estimates are much worse (Figure 15), especially near the frequencies $\Omega_0 = \pi m$, where the total energy is minimum valued. It will be shown in section 4 that when the loss factor and other energy characteristics are estimated in frequency bands, the estimation accuracy improves considerably.

3.3. A FLEXURALLY VIBRATING RECTANGULAR PLATE

As the last example, consider a thin rectangular plate flexurally vibrating under the action of an external point load (Figure 9(b)). It is assumed that the vibrational motion of the plate is governed by the classical equation of Germain–Lagrange [10] with a complex Young's modulus (23), and that all four sides of the plate are simply supported. For this structure, an analytical solution based on the expansion into the normal modes is available in the literature (e.g., in reference [11]). The necessary mathematics is outlined in Appendix B, while in this section the graphical material is presented. Again, two extreme cases of loading, force and velocity excitation, are considered separately. The results presented in Figures 16

and 17 correspond to the plate of dimensions $b/a = 1{\cdot}3$, to the load applied to the point $(0{\cdot}2a,\ 0{\cdot}3b)$, and to the material loss factor equal to $\eta_0 = 0{\cdot}05$.

As can be seen from Figures 16 and 17, the main features of the estimates (12)–(21) for the energy characteristics of the plate vibration manifest themselves just in the same manner as they do in the more simple structures studied above. Figure 16 is obtained for the case of force excitation. The velocity response as well as the total energy have maxima at the natural frequencies (resonances), which are separated by the minima at the anti-resonance frequencies. The estimate (13) via the input impedance (dotted line in Figure 16(b)) works well at low frequencies and at the resonance frequencies but fails at the anti-resonances. In the case of velocity excitation, when the point $(0{\cdot}2a,\ 0{\cdot}3b)$ has the prescribed velocity amplitude v_0, the response of the plate has maxima at the anti-resonance

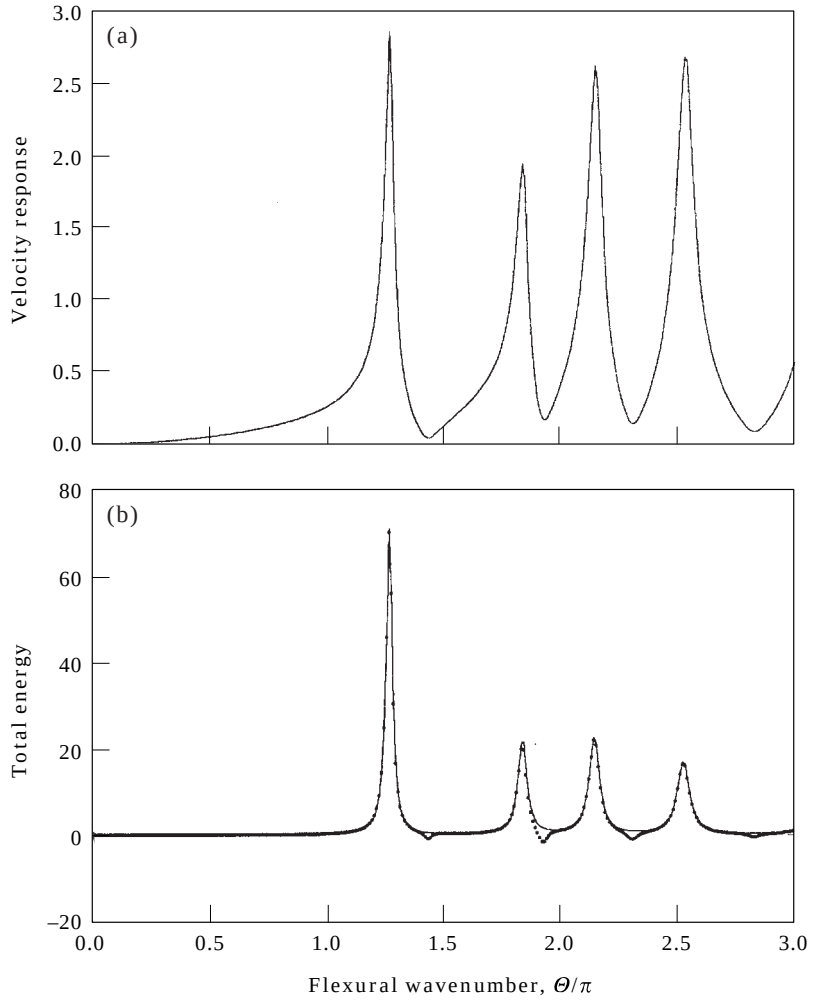

Figure 16. The velocity response at the driving point (a) and time-average total energy (b) of the forced vibrating plate: exact values (solid lines) and estimates via the input impedance (dots). The velocity is normalized with $|f/(B\rho h)^{1/2}|$, the total energy is normalized with the quantity $|f|^2/(Bab\pi^4)$, $B = E_0 I/a^4$.

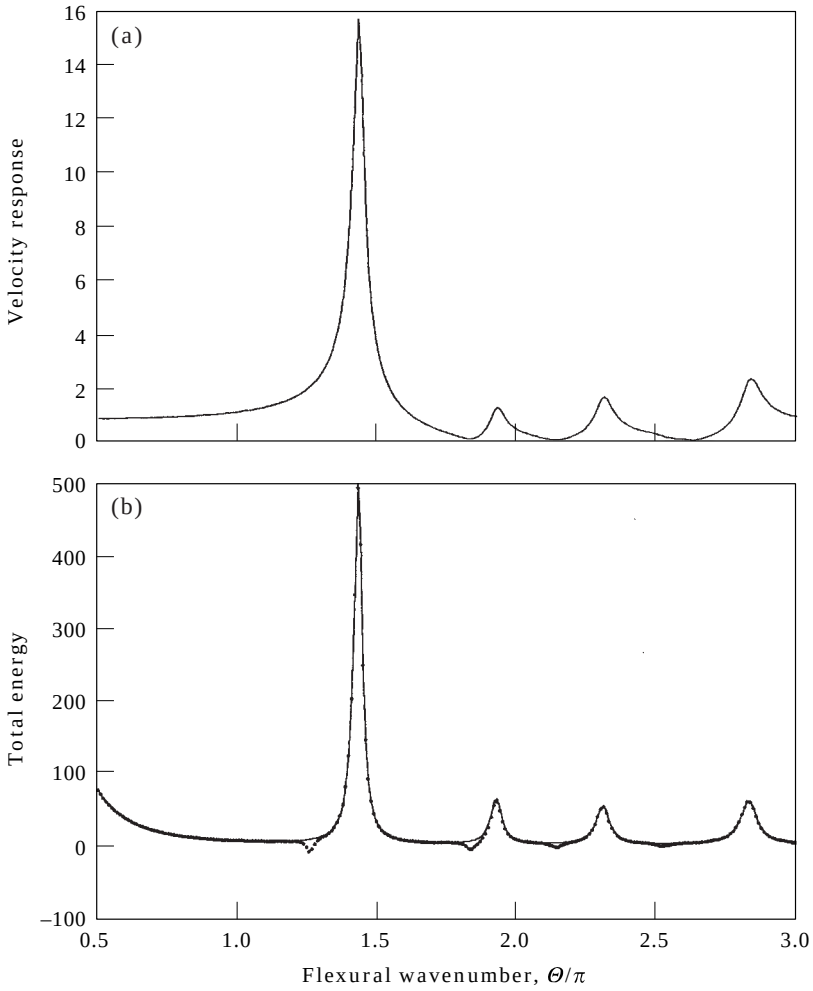

Figure 17. The velocity response at point (0·5a, 0·5b) normalized with $|v_0|$ (a) and the time-average total energy (b) of the plate kinematically excited at point (0·2a, 0·3b): exact values (solid lines) and estimates via the input mobility (dots). The total energy is normalized with $M|v_0|^2\pi^4/16$, where $M = \rho hab$ is the plate mass.

frequencies (Figure 17) and does not notice the resonance frequencies. The estimate (18) via the input mobility for the total energy (as well as for other energy characteristics not shown here) is the best in this case of loading, as clearly seen in Figure 17(b) (dotted line).

It follows from these results that estimation via the input impedance and mobility of the energy characteristics in a vibrating plate, as a two-dimensional structure, is just similar to estimation in one-dimensional structures and in mechanical systems with lumped parameters, at least at low and middle frequencies.

4. ANALYSIS OF THE RESULTS

4.1. BEHAVIOR OF THE ESTIMATES NEAR THE NATURAL FREQUENCIES

The examples of computer simulation of section 3 clearly show that the estimates via the input impedance work well at all frequencies but the frequencies of anti-resonance, and the estimates via the input mobility give a good approximation to the energy characteristics in a wide frequency range with the exception of the frequencies of resonance. This is the main feature of the proposed estimates, which exhibits itself in discrete mechanical systems as well as in continuous elastic structures. The explanation of the feature is the following.

First of all, it is worth recalling that if a linear mechanical system is driven by an external force at one point, the maximum response (resonance) of the system occurs at the natural frequencies of the system with the driving point free of tension, and the minimum response (anti-resonance) takes place at the natural frequencies of the system with the fixed driving point. For systems without damping, the resonance and anti-resonance frequencies interchange (between any two resonance frequencies there is an anti-resonance frequency, and between any two anti-resonances there is a resonance), so that the slope of the frequency response function never changes its sign in all the frequency range, except the resonance frequencies where the function jumps from $-i\infty$ to $+i\infty$. This result, known in the theory of electric circuits as Foster's theorem, is also valid for mechanical systems [11,12] and explains why the vibrational energy characteristics relate to the geometric property of the frequency response function as stated by the estimates under consideration.

It is also known [11] that near an isolated resonance, i.e., in a vicinity of a natural frequency, a mechanical system can be modelled by a simple resonance contour (Figure 18(a)) with m, k, c being the corresponding natural mode mass,

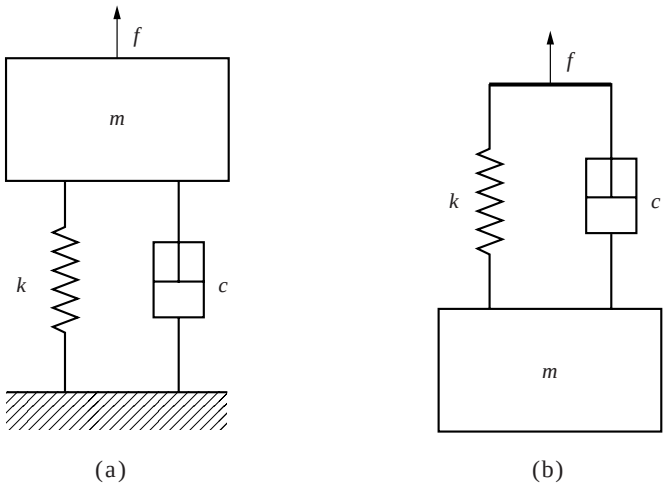

Figure 18. Simplified models of a linear structure which is forced vibrating near an isolated resonance (a) or anti-resonance (b).

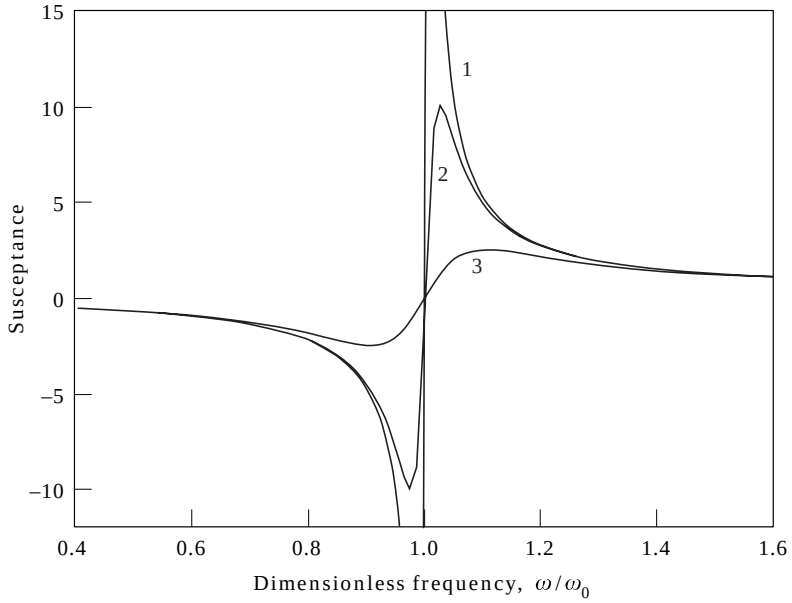

Figure 19. Imaginary part of the input mobility (susceptance) of the resonance contour; the loss factor is equal to $\eta = 0$ (curve 1), $\eta = 0{\cdot}05$ (2), $\eta = 0{\cdot}2$ (3).

stiffness, and damping parameters, with an external load being applied to the mass. The input impedance of this contour is equal to

$$z(\omega) = c + \mathrm{i}(k/\omega - \omega m) = m\omega_0[\eta + \mathrm{i}(1/\epsilon - \epsilon)], \tag{28}$$

where ω_0 is the resonance frequency, η is the loss factor, and $\epsilon = \omega/\omega_0$ is the dimensionless frequency. It is obvious that the imaginary part of the input impedance, the reactance, does not depend on the amount of damping c, and its value for a damped system is just the same as for the corresponding lossless system. For this reason, the energy estimate (13) via the input impedance, which is mathematically correct for lossless systems, will also be correct for damped systems. This explains the good approximation of the estimate (13) near resonances.

At the same time, the input mobility of the contour in Figure 18(a), i.e., the inverse of the input impedance (28), $y(\omega) = 1/z(\omega)$, depends a great deal on the damping, its imaginary part being equal to

$$\mathrm{Im}\,[y(\omega)]m\omega_0 = -(1/\epsilon - \epsilon)/[\eta^2 + (1/\epsilon - \epsilon)^2].$$

The graph of this function is plotted in Figure 19 for various values of the contour loss factor. It is seen from the figure that, at some distance from the natural frequency $\epsilon = 1$, the imaginary part of the input mobility of a damped contour does not differ from that of the lossless contour, but at the nearest proximity to the natural frequency the difference becomes drastic, the slope of the curve even changing its sign. This is an explanation of why the estimates via the input mobility do not work at the resonance frequencies and give negative values for the energy.

This also explains the fact that the width of the frequency band where these estimates fail is proportional to the amount of damping in the system.

In the vicinity of an anti-resonance frequency, the mechanical system under study can be modelled by a parallel contour (Figure 18(b)) with an external load being applied to the spring–dashpot connection. A reader can easily verify that, in this case, the imaginary part of the input mobility of the damped parallel contour is almost independent of the amount of damping (and does not differ from that of the contour without damping), while the imaginary part of the input impedance is strongly dependent on damping (the corresponding graph is very similar to that in Figure 19). This explains why the estimates via the input mobility work well at the anti-resonance frequencies and the estimates via the input impedance do not.

The conclusion is that the proposed estimates for the energy characteristics can fail only near some natural frequencies of the system, where the imaginary part of the input mobility or impedance is damping-controlled. At all other frequencies, including the low frequency range (from zero to the first natural frequency) and the regions between natural frequencies, the vibration response of the system is controlled by its reactive elements, and the estimates, both via the input impedance and mobility, give the approximations of high accuracy.

4.2. FREQUENCY RANGE OF VALIDITY

As is clear from the analysis presented above, the estimates under study can give good results only if the resonances and anti-resonances of the system are isolated from each other, i.e., if the distance along the frequency axis between adjacent

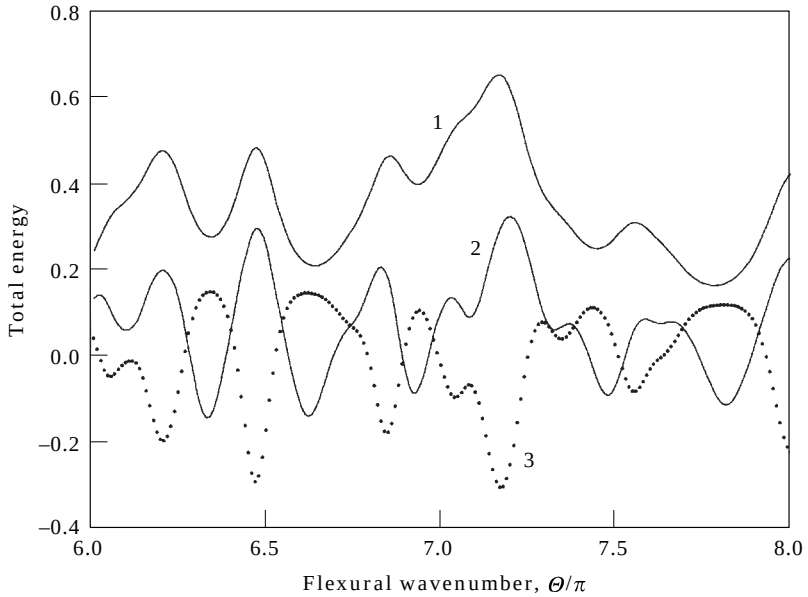

Figure 20. The total energy of the flexurally vibrating plate at high frequencies: 1—exact, 2—estimates via the input impedance, 3—estimate via the input mobility. The normalizing factor is as in Figure 16.

resonance and anti-resonance is greater than the width of the resonance peak. If that distance is comparable or smaller, both estimates via the impedance and mobility become invalid because of the destructive influence on each other. An example is presented in Figure 20. It corresponds to the high frequency flexural vibrations of the plate studied in section 3. In the frequency range of Figure 20, the density of the natural frequencies of the plate is such that, for the given material loss factor $\eta_0 = 0{\cdot}05$, the difference between adjacent resonances is an order of magnitude smaller than the resonance band width, and the overlapping resonances and anti-resonances produce a smooth frequency response, as shown by line 1 in Figure 20. Lines 2 and 3 in this figure represent the corresponding estimates through the input impedance and mobility. It is clearly seen that both the estimates do not work under such conditions. The range of validity for the proposed estimates, thus, comprises the frequencies ω which satisfy the inequality $\Delta\omega > \eta_0\omega$, where η_0 is the material loss factor, and $\Delta\omega$ is the mean distance between the adjacent resonances and anti-resonances which can be expressed through the density of the natural frequencies of the particular structure. For real structures of steel or aluminum having the loss factor $\eta_0 = 0{\cdot}01$–$0{\cdot}05$, the range of validity comprises low and middle frequencies.

4.3. ESTIMATION IN FREQUENCY BANDS

Among the energy characteristics investigated, the loss factor (7) has the lowest accuracy when estimated via the input impedance (16) or the input mobility (21)—see, e.g., Figures 6, 11 and 15. In this section it is shown that the accuracy can be remarkably improved if the estimation is made in a frequency band.

Consider, for example, the kinematically excited rod studied in section 3.2. The loss factor in a frequency band can be computed by summarizing the total and dissipated energy of all the harmonics in the band and using the general definition (7). Figures 21 and 22 present some results of the computation in 1/4- 1/2- and 1-octave bands. Ten equally spaced harmonics were taken into account in each band. Negative values of the total energy in the vicinity of resonance frequencies were replaced by zeros. Comparison of Figures 15 and 21 shows that the broader the frequency band, the better the estimate of the loss factor at low and middle frequencies: $\Omega_0 < 10$. The explanation of the increase in accuracy with the width of a frequency band is rather simple: the error in the estimated loss factor is caused by the error in the total energy estimation near certain natural frequencies where the energy itself has minimum values, the relative contribution of these values to the general level of the energy in the frequency band diminishes as the band width increases.

When the material loss factor decreases, the frequency range of validity becomes broader and the estimation accuracy gets better—see Figure 22 which corresponds to $\eta_0 = 0{\cdot}01$.

4.4. ROLE OF THE SOURCE TYPE

Accuracy of the proposed estimates is strongly dependent on the type of external excitation: for forced vibrating structures, the best approximation is provided by the estimates via the input impedance, and if a structure is kinematically excited

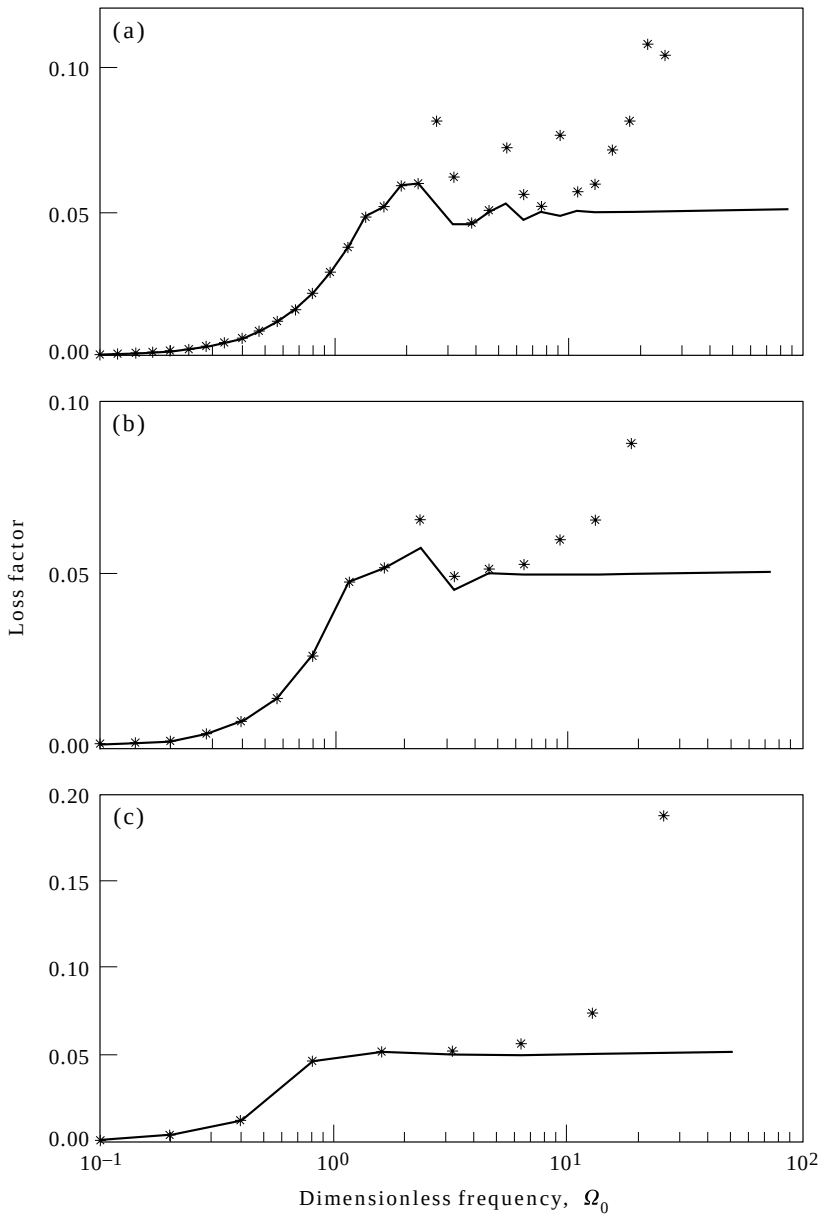

Figure 21. The loss factor of the kinematically excited rod in 1/4-octave (a), 1/2-octave (b), and 1-octave bands (c): solid lines correspond to exact values, stars designate estimates via the input mobility; the material loss factor is equal to 0·05.

the best are the estimates via the input mobility. In each case, before using the particular estimates, one has to verify the type of loading.

One way to do it practically is to measure the input impedance $z_s(\omega)$ of the non-operating source at the point of its attachment to the structure and compare it with the input impedance $z(\omega)$ of the structure. It should be emphasized that the comparison is necessary at the natural frequencies of the structure since these

are the only frequencies at which the estimates may fail. If the source impedance is much greater than the structure impedance, $|z_s(\omega)| \gg |z(\omega)|$, the source provides kinematic excitation of the structure. Such a situation occurs, for example, when a light-weighted structure is excited by a ceramic disk. Conversely, if the source impedance is much smaller than that of the structure, $|z_s(\omega)| \ll |z(\omega)|$, the force excitation is realized. An example is an electrodynamic shaker driving a massive structure. If the input impedances of the source and structure are of the same order

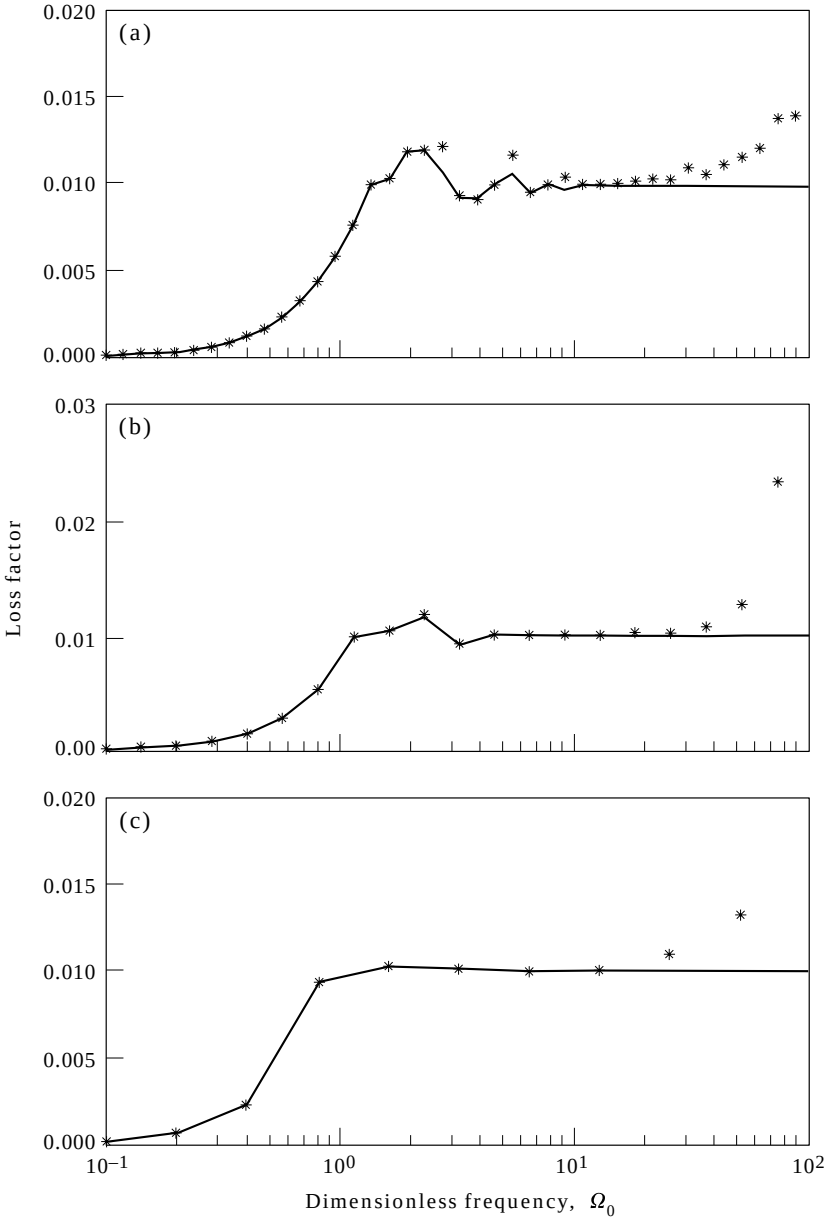

Figure 22. As Figure 21 for the material loss factor 0·01.

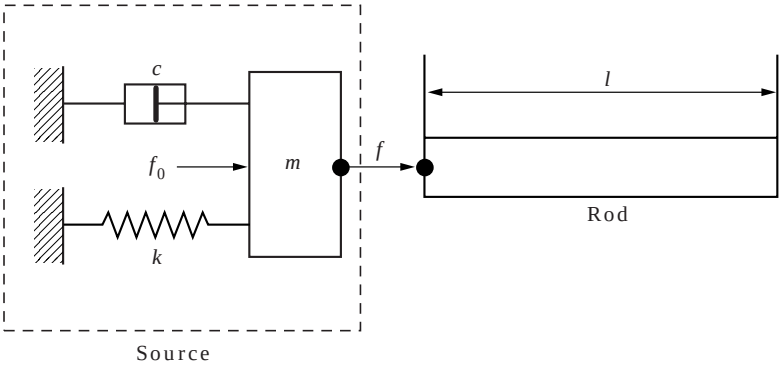

Figure 23. A rod excited by a source with an internal structure.

of magnitude, the general recommendation is to consider the coupled vibrations of the source–structure system.

As an example, consider the same rod as in section 3.2, which is excited this time by a source with a finite internal impedance. A schematic of the source is shown in Figure 23 (it represents a simplified model of a shaker). The internal force f_0 acts on the moving part of the shaker which is rigidly connected to the driven structure (rod). The amplitude f_0 is assumed to be independent of frequency.

The impedance of the rod $z(\omega)$ is given by equation (27) and the impedance of the source is (see equation (28)):

$$z_s(\omega) = z_{0s}[\eta + \mathrm{i}(\omega_0/\omega - \omega/\omega_0)], \tag{29}$$

where $z_{0s} = (mk)^{1/2}$ is the characteristic impedance of the source, $\omega_0 = (k/m)^{1/2}$ is the natural frequency, and $\eta = c/z_{0s}$ is the loss factor at the natural frequency ω_0.

The relation between the impedances of the source and structure is fully characterized by the impedance ratio in dB,

$$IR = 20 \lg |z(\omega)/z_s(\omega)|, \tag{30}$$

or, on average, by the ratio of the characteristic impedances

$$\beta = z_0/z_{0s}. \tag{31}$$

When β and IR are much greater than unity, the source is much more compliant than the rod and force excitation takes place. Figure 24 corresponds to $\beta = 100$ and to the source eigenfrequency $\Omega_\delta = \pi$. In this case, the rod impedance exceeds the source impedance by more than 20 dB at all the natural frequencies of rod (Figure 24(a)). It was directly verified that the driving force f is close to f_0 in all the frequency range (deviations are less than 6%); maximum response amplitudes take place at the resonance frequencies $\Omega_0 = \pi n$, and minimum response amplitudes occur at the anti-resonance frequencies $\Omega_0 = \pi n + \pi/2$. Consequently, the estimates via the input impedance give good results, as seen in Figure 24(b).

Figure 25 corresponds to the same source eigenfrequency and to the ratio (31) equal to $\beta = 0{\cdot}1$. In this case, the source is stiffer than the structure and all the anti-resonance frequencies $\Omega_0 = \pi/2$, $3\pi/2$ and $5\pi/2$ are excited: i.e., kinematic loading takes place. However, in the frequency band $\Omega_0 = 1$–5 the impedances are

of the same order (Figure 25(a)) and therefore the resonance frequency $\Omega_0 = \pi$ is also well excited. As a result, none of the two proposed estimates can provide a good approximation in all the frequency range: the estimate via the input impedance perfectly describes the resonance peak but fails at the anti-resonance frequencies, as is seen in Figure 25(b), while the estimate via the input mobility, conversely, describes well the peaks at the anti-resonance frequencies but gives erroneous results near the resonance $\Omega_0 = \pi$ (not shown in Figure 25(b)).

Here, one has a mixed case when the same source is of different types at various frequencies. To improve the situation, the internal structure of the source must be combined with the rod to form a complex structure with the force load f_0 (see Figure 23) to which one can apply the estimates via the input impedance and obtain necessary characteristics of this complex structure. This procedure, as well as the subsequent procedure of distinguishing between the energies of the source

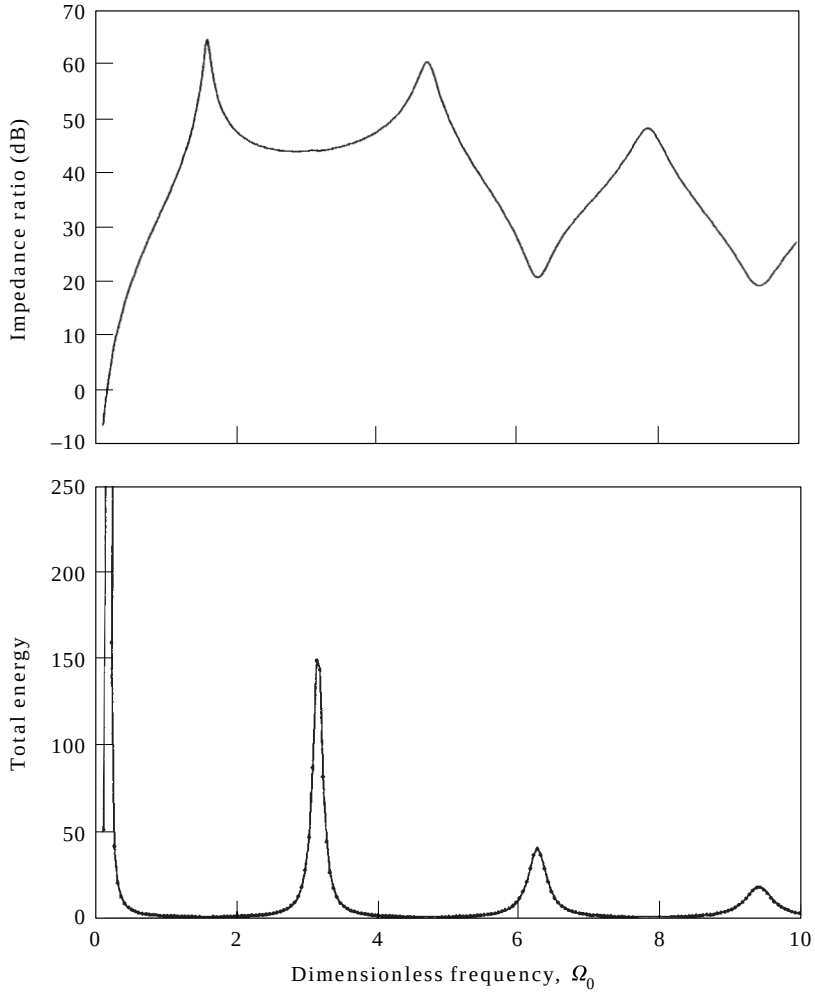

Figure 24. Impedance ratio (30) versus frequency for $\beta = 100$ (a) and the total energy estimate via the input impedance (dots) together with its exact values (solid lines) for the rod in Figure 23 (b). The internal eigenfrequency of the source is equal to $\Omega_0 = \pi$.

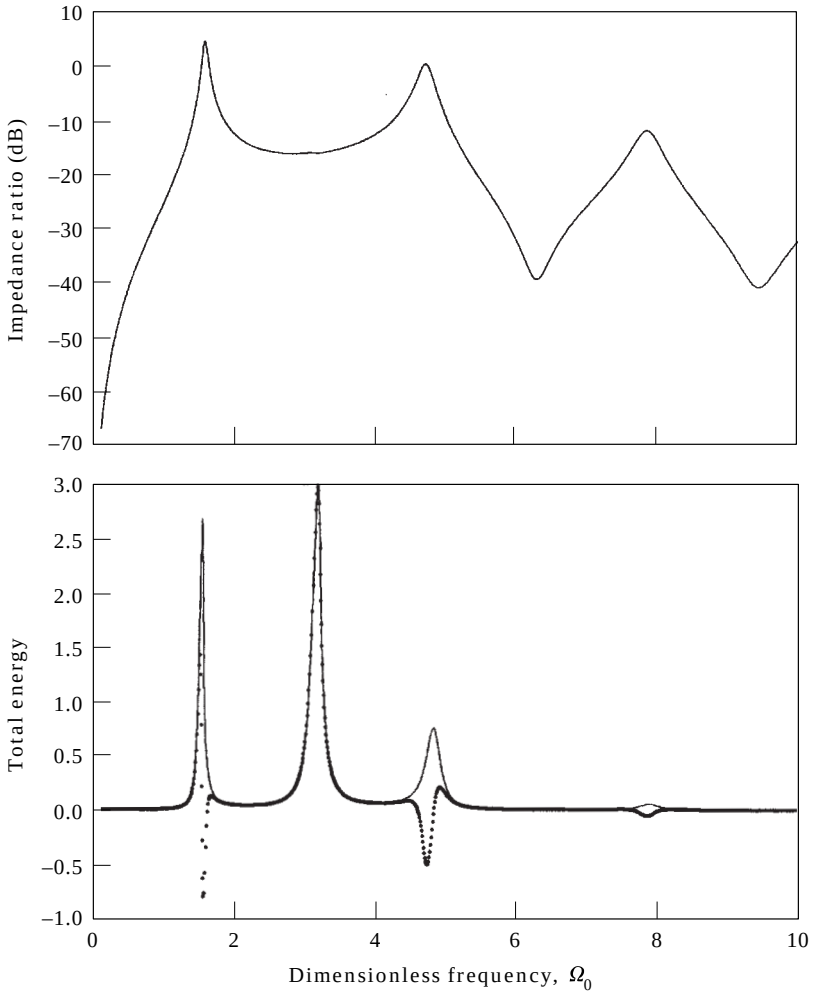

Figure 25. As Figure 24 for $\beta = 0{\cdot}1$.

and structure under study (rod), require a knowledge of a linear model of the source similar to that in Figure 23. Models for some sources used in vibration studies can be found in the literature, e.g., in reference [13], but for most mechanical sources of vibrations, machines in particular, adequate modelling is still a problem—see, e.g., references [14,15].

One more interesting observation: the proposed energy estimates normalized with the exact values do not depend on the type of the source. Figure 26 shows the frequency dependence of the energy estimate via the input impedance for the rod in Figure 23 normalized with the exact values of the energy. It was directly verified that the curve is invariant with the ratio (31): i.e., it does not depend on the impedance or other source characteristics, being a function of the rod parameters only. Figure 26 confirms once more that the estimate via the input impedance gives a large relative error only in narrow bands near the anti-resonance frequencies. However, the practical significance of the error is

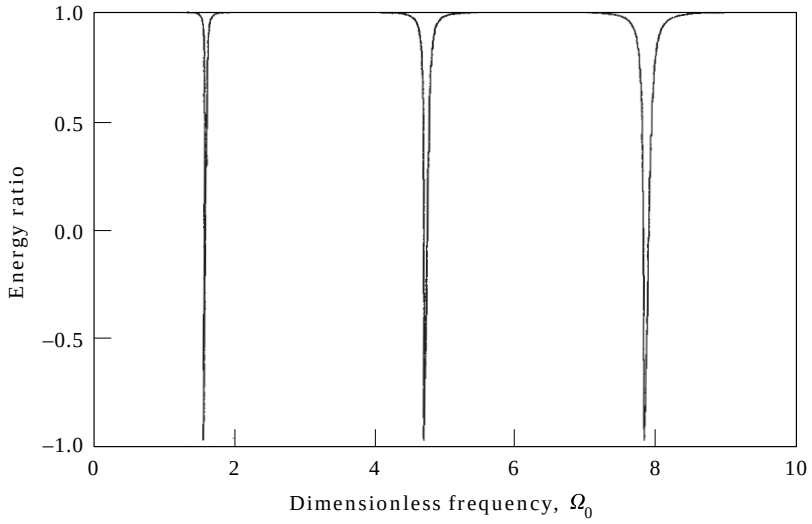

Figure 26. Estimate via the input impedance for the total energy of the rod normalized with the exact values.

different for different external loading: for excitation by a velocity source the error is principal as in Figure 25(b), and it is negligible for the force loading as in Figure 24(b).

5. CONCLUSIONS AND FURTHER DEVELOPMENTS

Several equations have been proposed in the present paper which allow one to estimate all the time-average vibration energy characteristics of a linear mechanical system driven at one point, by using only the data measured at the driving point. Computer simulation examples show that, for commonly used structures, these equations provide reliable estimates in the range of low and middle frequencies. They represent the most economic technique for estimating the energy characteristics of a structure since there is no need to measure or compute the vibrational response over the structure; even a structure model does not need to be known.

However, at the present stage, the proposed estimates have two serious drawbacks. First, the frequency range of validity is not as large as required, e.g., for SEA applications. Second, the estimates are now divided into two groups, one of which, based on using the input impedance, works best when the structure vibrates under force loading, while another group, based on using the input mobility, gives the best approximation for kinematically excited structures. So, a preliminary assessment of the type of external loading is required to choose between the two groups of the estimates before starting the estimation itself.

Meanwhile, some properties (such as this: when the first group fails the second group works best, and *vice versa*) indicate that there should exist combined estimates which accumulate the advantages of both groups, i.e., work equally well at resonances and anti-resonances. Such combined estimates would widen the

frequency range of validity and would be applicable to any type of external loading. Search for these estimates is one of the problems to be solved.

Practical implementation of the proposed estimates is obviously based on measurement of the input impedance or mobility and taking its derivative with respect to frequency. Since differentiation is an ill-posed operation very sensitive to the measurement errors, development of an appropriate impedance head and adequate differentiation technique for noisy data is another problem to focus on in the future.

ACKNOWLEDGMENT

This work was supported by the Russian Foundation for Basic Research: grant 98-01-00552a.

REFERENCES

1. V. V. Bolotin 1984 *Random Vibrations of Elastic Systems*. The Hague: Martinus Nijhoff.
2. D. J. Ewins 1997 *Proceedings of the* 6*th International Conference on Recent Advances in Structural Dynamics*, *Southampton*, *UK*, *Keynote Lecture*, 1–17. Recent advances in modal testing.
3. Yu. I. Bobrovnitskii 1997 *Proceedings of the* 6*th International Conference on Recent Advances in Structural Dynamics*, *Southampton*, *UK*, 1719–1731. The problem of expanding the vibration field from the measurement surface to the body of an elastic structure.
4. N. I. Prigorovsky 1983 *Methods and Means of Determining the Strain and Stress Fields*: *Handbook*. Moscow: Mashinostroenie (in Russian).
5. H. Ahmadian, G. M. L. Gladwell and F. Ismail 1994 *Journal of Sound and Vibration* **172**, 657–669. Finite element model identification using modal data.
6. M. J. Schulz and D. L. Inman 1994 *Journal of Sound and Vibration* **178**, 113–130. Model updating using constrained eigenstructure assignments.
7. Yu. I. Bobrovnitskii 1989 *Proceedings of the* 13*th International Congress on Acoustics*, *Belgrade*, *Yugoslavia* **3**, 389–392. Energy relations for acousto-structural waveguides.
8. Yu. I. Bobrovnitskii 1997 *Proceedings of the IUTAM Symposium on SEA* (editor F. J. Fahy) *Southampton*, *U.K.* Some energy relations for mechanical systems.
9. F. J. Fahy and H. M. Ruivo 1997 *Journal of Sound and Vibration* **203**, 763–779. Determination of statistical energy analysis loss factors by means of an input power modulated technique.
10. K. F. Graff 1975 *Wave Motion in Elastic Solids*. Oxford: Clarendon Press.
11. E. Skudrzyk 1968 *Simple and Complex Vibratory Systems*. University Park and London: The Penn State University Press.
12. S. Karni 1966 *Network Theory*: *Analysis and Synthesis*. Boston, MA: Allyn and Bacon, Inc.
13. E. Skudrzyk 1971 *The Foundations of Acoustics*. Wien: Springer-Verlag.
14. H. G. D. Goyder and R. G. White 1980 *Journal of Sound and Vibration* **68**, 97–117. Vibrational power flow from machines into built-up structures, part III: power flow through isolation systems.
15. R. A. Fulford and B. M. Gibbs 1997 *Journal of Sound and Vibration* **204**, 659–677. Structure-borne sound power and source characterization in multi-point-connected systems.

16. K. A. INGEBRIGTSEN and A. TONNING 1969 *Physical Review* **184**, 942–951. Elastic surface waves in crystals.
17. YU. I. BOBROVNITSKII and V. V. TYUTEKIN 1986 *Soviet Physics Acoustics* **32**, 373–379. Energy characteristics of composite waveguides.

APPENDIX A: DERIVATION OF EQUATIONS (13) AND (18)

Equation (13), which relates the time-average vibration energy of a linear mechanical system to the derivative of its input impedance with respect to frequency, is not entirely new. A similar equation is known in the theory of electric circuits as the theorem about a reactive twopole [12]: for a twopole consisting of linear reactive elements, the reactance is proportional to the difference between the energy of the magnetic field and the energy of the electric field (compare with equation (12)), and the derivative of the reactance with respect to frequency is proportional to the sum of these energies, i.e., to the total electro-magnetic energy of the circuit. A similar result is also known in the theory of acoustic surface waves (see, e.g., reference [16]): the total energy per unit area in the Rayleigh wave in a semi-infinite anisotropic solid medium can be expressed in terms of the displacement amplitude and the derivative of the impedance of the boundary surface of the halfspace. In reference [17], this result is extended to compound waveguides consisting of two or several interacting uniform subsystems (e.g., a cylindrical shell with a fluid): energy of each subsystem is proportional to the derivative of the subsystem impedance defined on the interaction surfaces.

Among the results cited, the closest to equation (13) is the result of the electric circuit theory. In principle, by using the electro-mechanical analogy [11], the theorem about a reactive twopole could be expanded to lossless mechanical nDOF systems. However, the proof of the theorem about twopoles is based upon Kirchhoff's equations and some other results of the electric circuit theory which are not used in the theory of mechanical vibrations.

Therefore below, for mechanical nDOF systems, equation (13) as well as equation (18), which has no analogs in the literature, are derived by the direct method suggested in reference [7] which uses only the concepts of mechanics and the theory of matrices.

We start the derivation from the following statement: for an arbitrary linear nDOF-system, if one knows the full impedance $n \times n$-matrix $\mathbf{Z}$ and the full velocity response n-vector $\mathbf{v}$ in equation (1), then the time-average total energy of the system is equal to

$$E = -\tfrac{1}{4}[\mathbf{v}^{(n)}]^* \frac{\partial \mathbf{X}^{(n)}}{\partial \omega} \mathbf{v}^{(n)}, \tag{A1}$$

where $\mathbf{X}^{(n)} = \text{Im}\, \mathbf{Z}^{(n)}$. The upper index n is introduced here for the velocity vector, impedance matrix, and reactance matrix to emphasize their dimensions. The validity of equation (A1) is immediately established by substitution into it of equation (2). It is not assumed from the very beginning that there is no damping in the system. Equation (A1) is evidently valid for any nDOF-system, lossless

or damped. Equation (A1) holds for all possible external forcing, including the case we are interested in, namely, the case when the system is driven only at the first DOF: $f_1 = f$; $f_2 = f_3 = \cdots = f_n = 0$.

The next step is to reduce by one the dimension of the sum in equation (A1) by using the condition that the nth component of the force vector is equal to zero:

$$f_n = \sum_{j=1}^{n} Z_{nj}^{(n)} v_j = 0.$$

Expressing from this equation the velocity component v_n through the rest of the velocity components and substituting it into equations (1) and (A1) leads to the equations

$$\mathbf{f}^{(n-1)} = \mathbf{Z}^{(n-1)}\mathbf{v}^{(n-1)}, \tag{A2}$$

$$E = -\frac{1}{4}\sum_{j,k=1}^{n-1} v_j A_{jk}^{(n-1)} v_k = -\frac{1}{4}[\mathbf{v}^{n-1)}]^{*}\mathbf{A}^{(n-1)}\mathbf{v}^{(n-1)}, \tag{A3}$$

where $\mathbf{Z}^{(n-1)}$ is the input impedance $(n-1)\times(n-1)$-matrix of the system defined with respect to the first $(n-1)$ degrees of freedom. Its elements are expressed via the elements of the full impedance matrix $\mathbf{Z}^{(n)}$ as

$$Z_{jk}^{(n-1)} = Z_{jk}^{(n)} - \frac{Z_{jn}^{(n)} Z_{nk}^{(n)}}{Z_{nn}^{(n)}}. \tag{A4}$$

Elements of $(n-1)\times(n-1)$-matrix $\mathbf{A}^{(n-1)}$ in equation (A3) are also expressed through the elements of the full matrices $\mathbf{Z}^{(n)}$ and $\partial\mathbf{X}^{(n)}/\partial\omega$ as

$$A_{jk}^{(n-1)} = \frac{\partial X_{jk}^{(n)}}{\partial\omega} - \frac{Z_{jn}^{(n)}}{Z_{nn}^{(n)}}\frac{\partial X_{nk}^{(n)}}{\partial\omega} - \frac{\partial X_{jn}^{(n)}}{\partial\omega}\frac{Z_{nk}^{(n)}}{Z_{nn}^{(n)}} + \frac{Z_{jn}^{(n)} Z_{nk}^{(n)}}{|Z_{nn}^{(n)}|^2}\frac{\partial X_{nn}^{(n)}}{\partial\omega}. \tag{A5}$$

The key point of the derivation is to find out under what conditions equation (A3) for the total energy relates to the input impedance matrix (A2) exactly as equation (A1) relates to the full impedance matrix (1), or, in other words, when element (A5) is equal to the derivative of the imaginary part of element (A4) with respect to frequency:

$$A_{jn}^{(n-1)} = \frac{\partial}{\partial\omega}[\mathrm{Im}\ Z_{jk}^{(n-1)}]. \tag{A6}$$

Detailed analysis shows that equation (A6) is valid if and only if the elements of the full impedance matrix (1) are pure imaginary, that is to say, if the nDOF-system under study is lossless: $\mathbf{H} = \mathbf{C} = \mathbf{0}$. In that case, the total energy of the system E can be expressed through the derivative of the input impedance matrix of order $(n-1)$:

$$E = -\tfrac{1}{4}[\mathbf{v}^{(n-1)}]^{*}\frac{\partial\mathbf{X}^{(n-1)}}{\partial\omega}\mathbf{v}^{(n-1)}. \tag{A7}$$

Thus, for lossless nDOF-systems, it is possible to reduce by one the number of the velocity responses v_j (or degrees of freedom) involved in computing the total energy of the system.

Starting from equations (A2) and (A7), which have dimension $(n-1)$, and excluding the velocity component v_{n-1} from the condition $f_{n-1}=0$, one can in a similar manner further reduce the dimension of equations (A2) and (A7) by one and obtain the equations

$$\mathbf{f}^{(n-2)} = \mathbf{Z}^{(n-2)}\mathbf{v}^{(n-2)}, \qquad E = -\tfrac{1}{4}[\mathbf{v}^{(n-2)}]^* \frac{\partial \mathbf{X}^{(n-2)}}{\partial \omega}\,\mathbf{v}^{(n-2)}. \qquad \text{(A8, A9)}$$

Here the $(n-2)$-vectors $\mathbf{f}^{(n-2)}$ and $\mathbf{v}^{(n-2)}$ are composed of the first $(n-2)$ components of the full force and velocity response vectors $\mathbf{f}^{(n)}$ and $\mathbf{v}^{(n)}$, $\mathbf{Z}^{(n-2)}$ is the $(n-2)\times(n-2)$-matrix of the input impedances of the system with elements

$$Z_{jk}^{(n-2)} = Z_{jk}^{(n-1)} - \frac{Z_{j,n-1}^{(n-1)} Z_{n-1,k}^{(n-1)}}{Z_{n-1,n-1}^{(n-1)}},$$

and $\mathbf{X}^{(n-2)}$ is the imaginary part of the matrix $\mathbf{Z}^{(n-2)}$. Again, this procedure of reducing dimension is possible only for lossless systems with $\mathbf{Z}^{(n-2)} = \mathrm{i}\mathbf{X}^{(n-2)}$.

Continuing the process, one can, by induction, exclude the velocity components of all DOFs free of external forcing and obtain equations of type (A8) and (A9) for any dimension k: $1 \leqslant k \leqslant n$. In the limiting case of $k=1$, one comes to the required result (13):

$$f_1 = Z^{(1)} v_1, \qquad E = -\tfrac{1}{4}|v_1|^2 \frac{\partial X^{(1)}}{\partial \omega}, \qquad \text{(A10)}$$

where $Z^{(1)} = z(\omega)$ is the scalar input impedance at the first DOF of the system, and $v_1 = v$.

Equation (18), which relates the total energy to the input mobility $y(\omega) = 1/z(\omega)$, can easily be obtained by taking into account the equality $[y(\omega)]^2 = -|y(\omega)|^2$ (the system is lossless and the mobility is pure imaginary) and starting from equation (A10):

$$E = -\tfrac{1}{4}|f_1|^2 \,\mathrm{Im}\left[\frac{\partial y(\omega)}{\partial \omega}\right]. \qquad \text{(A11)}$$

APPENDIX B: FORCED VIBRATING SIMPLY SUPPORTED RECTANGULAR PLATE

In this appendix, a solution for a flexurally vibrating plate is presented which is used in section 3.3 for plotting the graphs of Figures 16 and 17.

A thin rectangular uniform plate performs flexural vibrations under the action of a point load (Figure 9(b)). The thickness, width, and length of the plate are h, a, and b. Young's modulus of the material is complex—see equation (23). An

external force of complex amplitude f is applied to point (x_0, y_0). The lateral displacement $w(x, y)$ of the plate satisfies the classical equation [10]

$$E_c I \Delta^2 w(x, y) - \rho h \omega^2 w(x, y) = f \delta(x - x_0)\delta(y - y_0) \tag{B1}$$

and the boundary conditions

$$w(0, y) = w(a, y) = w(x, 0) = w(x, b),$$

$$\frac{\partial^2 w}{\partial x^2} + \nu \frac{\partial^2 w}{\partial y^2} = 0|_{x=0,a}, \qquad \frac{\partial^2 w}{\partial y^2} + \nu \frac{\partial^2 w}{\partial x^2} = 0|_{y=0,b}. \tag{B2}$$

Natural frequencies and the corresponding normal modes, which satisfy the homogeneous equation (B1) and conditions (B2), are

$$\omega_{mn} = \left[\left(\frac{\pi m}{a}\right)^2 + \left(\frac{\pi n}{b}\right)^2\right]\sqrt{\frac{E_0 I}{\rho h}}, \qquad w_{mn}(x, y) = \frac{2}{\sqrt{ab}} \sin\frac{\pi m x}{a} \sin\frac{\pi n y}{b}, \tag{B3, B4}$$

where m, n are natural numbers, the normal modes (B4) being orthogonal:

$$\int_0^a \int_0^b w_{mn}(x, y) w_{pq}(x, y)\, \mathrm{d}x\, \mathrm{d}y = \delta_{mp}\delta_{nq}. \tag{B5}$$

The solution of the forced vibration problem is sought in the form of an expansion in the normal modes:

$$w(x, y) = \sum_{m=1}^{\infty} \sum_{n=1}^{\infty} \gamma_{mn} w_{mn}(x, y). \tag{B6}$$

Substituting equation (B6) into equation (B1) and using equations (B3)–(B5) leads to the following equation for the expansion coefficients:

$$\gamma_{mn} = \frac{f a^4}{E_0 I} \frac{w_{mn}(x_0, y_0)}{D_{mn}}, \qquad D_{mn} = \Theta_{mn}^4 - \Theta^4 - \mathrm{i}\eta\Theta_{mn}^4. \tag{B7, B8}$$

Here $\Theta = k_f a$ is the dimensionless flexural wavenumber proportional to the square root of frequency ($k_f^4 = \rho h \omega^2 / E_0 I$) and $\Theta_{mn} = \pi(m^2 + n^2/\alpha^2)^{1/2}$ is the value of Θ at the natural frequency (B3), $\alpha = b/a$.

The exact values of the energy characteristics (4)–(7) are computed by using the solution (B6) with a finite number of the terms. For example, the kinetic and potential energies are respectively

$$T = \tfrac{1}{4}\rho h \omega^2 \int_0^a \int_0^b |w(x, y)|^2\, \mathrm{d}x\, \mathrm{d}y = \frac{|f|^2 a^4 \Theta^4}{4 E_0 I} \sum_{m=1}^{M} \sum_{n=1}^{N} \frac{w_{mn}^2(x, y)}{|D_{mn}|^2}, \tag{B9}$$

$$U = \tfrac{1}{4}E_0 I \int_o^a \int_0^b \left\{ |\Delta w|^2 + 2(1-\nu)\left[\left| \frac{\partial^2 w}{\partial x\, \partial y} \right| - \mathrm{Re}\left(\frac{\partial^2 w}{\partial x^2} \frac{\partial^2 w}{\partial y^2} \right) \right] \right\} \mathrm{d}x\, \mathrm{d}y$$

$$= \frac{|f|^2 a^4}{4E_0 I} \sum_{m=1}^{M} \sum_{n=1}^{N} \frac{\Theta_{mn}^4 w_{mn}^2(x_0, y_0)}{|D_{mn}|^2}. \tag{B10}$$

The input mobility of the plate is

$$y(\omega) = -\frac{\mathrm{i}\omega a^4}{E_0 I} \sum_{m=1}^{M} \sum_{n=1}^{N} \frac{w_{mn}^2(x_0, y_0)}{D_{mn}}, \tag{B11}$$

and the input impedance is calculated as the inverse of this expression.

The solution for the kinematic excitation (when at the driving point the velocity amplitude v_0 is prescribed) can be obtained from the solution (B6)–(B10) by replacing the force amplitude f by the quantity $v_0/y(\omega)$.

The expansion coefficients (B7) as well as the terms in the series (B10) and (B11) decay very rapidly with m and n (as m^{-4} and n^{-4}) and for the kinetic energy (B9) the decay is even more rapid—as m^{-8} and n^{-8}. All the series (B6)–(B11) thus have very good convergence and, in computing the characteristics of the flexural vibration field, it is sufficient to limit the number of the normal modes involved by 100: $M = N = 10$.

APPENDIX C: LIST OF SYMBOLS

a, b	plate edge lengths
$\mathbf{C}, c, c_j$	viscous damping matrix and coefficients
E	time-average total energy
E_c, E_0	complex and real Young's modulus
$\mathbf{F}, F$	complex power flow
$\mathbf{f}, f, f_j$	external force vector and components
$\mathbf{H}$	matrix of hysteretic damping
i	imaginary unit
$\mathbf{K}, k, k_j$	static stiffness matrix and coefficients
L	Lagrange function
l	rod length
$\mathbf{M}, m_j$	mass matrix and coefficients
M, m, N, n	natural numbers
T, U	time-average kinetic and potential energy
$u(x)$	rod displacement
$\mathbf{v}, v_j, v_0$	velocity vector and components
$w(x, y)$	plate displacement
$\mathbf{X}$	reactance matrix
$y(\omega), z(\omega)$	input mobility and impedance
$\mathbf{Z}$	impedance matrix
α	plate aspect ratio b/a
$\delta(\cdot)$	Dirac delta function
δ_{mn}	Kronecker's symbol
Φ	time-average dissipated power

η, η_0	structure and material loss factor
ν	Poisson's ratio
Θ	dimensionless flexural wavenumber
ρ	material density
ω	circular frequency
Ω, Ω_0	complex and real dimensionless longitudinal wavenumber